Construct Innovate
Built Environment Research Ireland

Alternative Irish-based materials suitable as cementitious binders

April 2026

Construct Innovate

Peer Reviewed document

Alternative Irish-based materials suitable as cementitious binders

Author: Dr Niall Holmes
Construct Innovate RPO: Technological University Dublin

Construct Innovate greatly values the work of the reviewers as their expert knowledge greatly contribute to the high standards of the Construct Innovate publications, therefore Construct Innovate thank the reviewers for their participation.

This technical report is a part of 2024 Seed Fund CISFC1-24_008: Alternative Irish-based materials suitable as cementitious binders Project and it has been Peer Reviewed through Construct Innovate in April 2026.

Project Acronym	Alternative Irish SCMs
Project Name	Alternative Irish-based materials suitable as cementitious binders
Project Coordinator	Dr Niall Holmes +353 87 069 6211
Project Duration	12 Months (starting January 2025).
Website	https://constructinnovate.ie/2024/06/alternative-materials-cementitious-binders

Deliverable No.	Final Deliverable
Dissemination Level	Public
Work Package	1
Lead Beneficiary	TU Dublin
Contributing Beneficiary	Arup Consulting Engineers, Breedon Concrete, McGraths quarries, FutureCast, Mannok Build & Sisk contractors.

Version	Date	Modifications
v1.01	04/12/2025	

Contents

1 Introduction 5

1.1 The need for alternative cement-based materials 5

1.2 Cement and concrete production in Ireland 6

Cement and Concrete Output in Ireland 6

CO_2 Emissions from Cement Manufacture 6

Trends & Recent Changes 6

Policy and Decarbonisation Efforts 7

1.3 Aims and objectives of this project 7

1.4 Project Partners 8

2 Sources of SCMs 9

Fly-ash and Bottom Ash 9

GGBS 10

Recycled Glass Powder 11

Calcined clays 12

Red mud 13

Aughinish Alumina 14

Geoploymer 14

3 SCM Characterisation 16

3.1 XRF Analysis 16

3.2 XRD analysis 18

CEM I and CEM II / A-L 19

PFA 19

GGBS 22

FBA 23

RGP 24

Calcined Clay 26

4 Concrete Compressive Strengths 27

Materials 27

Preparation of samples 27

4.1 Compressive Strength results 29
5 Thermodynamic modelling 33
OPC Normative Calculation 34
OPC Clinker Rate Equations 34
Dissolution of Oxides Dissolved in OPC Clinker 35
Accessory Clinker Phases 35
Oversaturation 36
Alkalis binding to the C-S-H 36
Hydrogarnet Solid Solution 37
Full hydration analysis 37
CEM I and CEM II A/L cement models 37
PFA models 38
FBA models 40
GGBS models 40
RGP models 41
Red Mud models 42
Geopolymer model 44
5.2 Phase assemblage predictions 45
CEM I and CEM II / A-L 45
PFA 45
FBA 46
GGBS 47
RGP 47
Calcined Clay 48
Red mud 49
6 Route to standardisation 51
7 Discussion and Conclusions 53
7.1 Experimental findings 53
7.2 Challenges, Considerations and the Path Forward 53

1 Introduction

1.1 The need for alternative cement-based materials

The production and use of conventional Portland cement underpin modern construction in Ireland and across the world. However, combined, they represent a significant challenge in the transition to a low-carbon built environment. Cement manufacture is one of the most carbon-intensive industrial processes globally, contributing approximately 8 % of worldwide CO_2 emissions[1] due to the high temperatures and chemical reactions required to produce clinker, the principal component of traditional cements. Approximately 60% of CO_2 arising from cement production is from the calcination of limestone with the remaining 40% from fuel combustion[2].

In response to escalating climate commitments outlined in national and European climate policy frameworks, there is growing urgency to reduce the embodied carbon of cementitious materials used in Irish construction. Recent government procurement reforms now explicitly aim to reduce the clinker content of cements used in public infrastructure projects by at least 30%[3] and exclude high carbon CEM I cement from public contracts, signalling a strategic shift toward lower-impact binders. This shift acknowledges that incremental improvements in existing cement formulations, while beneficial, will not be sufficient on their own to meet long-term decarbonisation targets.

Existing approaches in Ireland, such as the widespread use of CEM II eco-efficient cements[4] with modest clinker substitution and supplementary cementitious materials (SCMs), demonstrate continued progress toward lower carbon products. These products partially replace clinker with limestone or other materials, yielding reductions in carbon emissions without sacrificing performance. In addition, commercial low-carbon concrete solutions, such as Kilsaran's *ClimaKrete*[5], use SCMs like ground granulated blast furnace slag (GGBS) and other admixtures to deliver performance comparable to traditional concrete while reducing embodied carbon.

Snellings *et al*[6] investigated a wide range of natural and waste resources as potential SCMs, ranging from well-tried constituents emerging on the markets to materials still in initial stages of explorative research. Climate change mitigation along with waste reduction and upcycling objectives have sparked intense research activity in the field of SCMs for use as cements in concrete. Figure 1 compares the chemical composition of commonly used SCMs to the most relevant emerging and future SCMs.

Yet the availability and sustainability of conventional SCMs such as GGBS and pulverised fly ash are constrained by market and supply dynamics, and their future availability may decline as related industries decarbonise or close. This underscores a research gap in identifying new locally available or engineered alternatives that can sustain and expand low-carbon cement production in Ireland[7].

[1] https://www.weforum.org/stories/2024/09/cement-production-sustainable-concrete-co2-emissions/

[2] https://blog.sintef.com/energy/the-cemcap-framework-public-and-ready-for-use/

[3] https://www.gov.ie/en/department-of-enterprise-tourism-and-employment/press-releases/government-approves-public-procurement-guidance-to-promote-the-reduction-of-embodied-carbon-in-construction/

[4] https://www.irishcement.ie/eco-efficient-cem-ii-2/

[5] https://www.kilsaran.ie/climakrete/

[6] Snellings, R., Suraneni, P. and Skibsted, J., 2023. Future and emerging supplementary cementitious materials. Cement and concrete research, 171, p.107199.

[7] https://constructinnovate.ie/2025/05/commercialisation-of-low-carbon-cements

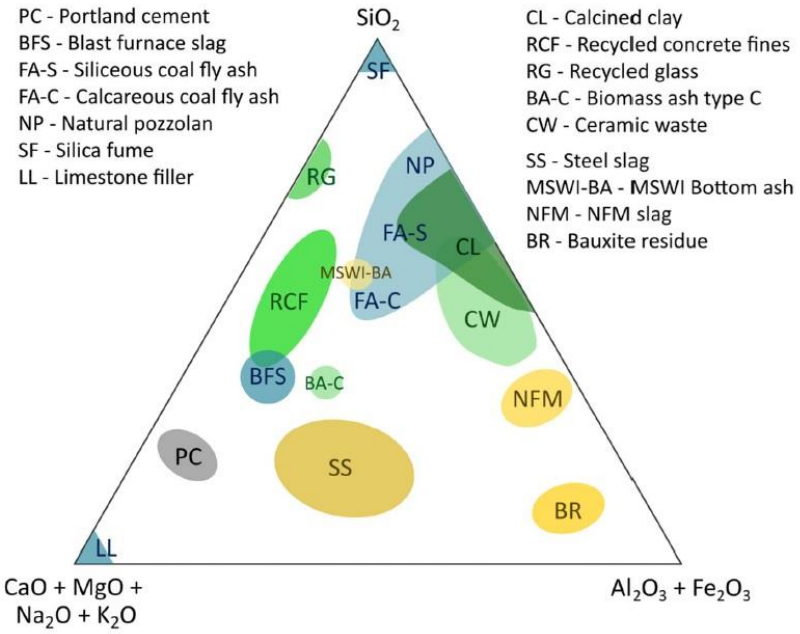

Figure 1 The chemical composition ranges of common, emerging and future SCMs in a ternary diagram of (earth)alkalis – silica – alumina/iron oxide taken from[6]

Developing alternative cements goes beyond environmental concerns; it also has economic and strategic dimensions. Innovation in binder technology could position the Irish cement sector at the forefront of sustainable material export markets and reduce reliance on imported cementitious products. However, such innovation must be underpinned by robust research that addresses technical performance, regulatory compliance, lifecycle impacts and scalability.

In essence, the transition toward alternative cements on the island of Ireland is not merely an academic exercise—it is a necessary component of national climate action, essential to decarbonising the construction sector while maintaining the integrity, durability, and affordability of critical infrastructure. Continued research and collaboration across academia, industry, and government will be critical to achieving these goals.

1.2 Cement and concrete production in Ireland

Below are a few facts and figures around cement and concrete production in Ireland with a particular focus on production levels, CO_2 emissions and future trends.

Cement and Concrete Output in Ireland

- Cement production is approximately 5 million tonnes per year
- Concrete production is estimated at 21 million tonnes per year
- Approximately half of Ireland's cement production is exported, with the majority to the UK market.

CO_2 Emissions from Cement Manufacture

- Approximately, 2.9 million tonnes of CO_2 are emitted from cement production, which represents around 5% of Ireland's total greenhouse gas emissions

Trends & Recent Changes

- Cement production emissions have varied over time rising from ~2.5 million tonnes of CO_2 in 2010 to

~3.6 million tonnes in 2022[8]

- Lower CO_2 emissions have been reported from the four main Irish cement plants to around 2.7 million tonnes in 2023[9]
- Lower cement industry CO_2 production has contributed to an overall reduction in industrial emissions[10]

Policy and Decarbonisation Efforts

- The Irish Government has mandated a 30% reduction in clinker content in public procurement of cement and concrete[11].

1.3 Aims and objectives of this project

This project studied several possible SCMs on the island of Ireland to partially replace cement in construction materials, including pulverised fly ash, China clay/ kaolin, red mud, furnace bottom ash and recycled powdered glass. A study in geopolymer concrete was also included but the compressive strength results were not ready in time for the report submission. A suite of experimental testing was undertaken on these SCMs to understand the underlying chemistry, behaviour during hydration and compressive strength. A suite of thermodynamic modelling was carried out to predict long-term hydration behaviour in terms of phase development and pH changes. An initial discussion with the NSAI into developing a roadmap for their standardisation was also held.

The main objectives of the project were to:

- Develop a database of potential SCMs detailing their resource potential.
- Undertake chemical and hydration study of new SCMs as partial cement replacements.
- Produce thermodynamic predictive models of long-term hydration and phase development.
- Test concrete samples incorporating the new SCMs for workability and strength performance.
- Liaise with the NSAI to develop a new roadmap for standardising new SCMs.

This is an important strategic project for the Irish cement and concrete sector and will be the first time a dedicated study on the potential sources of SCMs on the island of Ireland has been undertaken. It provides the location and potential of such source along with an understanding of their behaviour in cement-based materials. The outcome of this project includes locations of each material and their availability, chemical and hydration study data, thermodynamic input files, hardened concrete results and a roadmap for future standardisation. All results, data generated, reports, presentations, etc. are prime for exploitation by industry partners and fit perfectly within the scope of Impact 2030[12].

[8] Decoupling Emissions from Economic Activity 2022 (CSO website 19 November 2024)

[9] Climate Change Advisory Council (2024), Industry and Waste Sectoral Review: Annual Review 2024. https://www.climatecouncil.ie/councilpublications/

[10] EPA website Ireland's power generation and industrial emissions decreased by seventeen per cent in 2023

[11] https://www.gov.ie/en/department-of-enterprise-tourism-and-employment/press-releases/government-approves-public-procurement-guidance-to-promote-the-reduction-of-embodied-carbon-in-construction/

[12] https://www.gov.ie/en/department-of-further-and-higher-education-research-innovation-and-science/publications/impact-2030-irelands-research-and-innovation-strategy/

1.4 Project Partners

This project was carried out with the financial and technical support of the partners below.

Arup Consulting Engineers

Breedon Concrete

McGraths quarries

FutureCast

Mannok Concrete

Sisk contractors

RPS consulting Engineers

2 Sources of SCMs

Fly-ash and Bottom Ash

The ESB Moneypoint Generating Station (Figure 2) has been operating since 1985 and is located on Shannon estuary in County Clare. At its peak, its three coal-fired power generating units could produce up to 305 MW of electricity each supplying about a quarter of Ireland's total electricity needs.

The primary fuel used in the station is coal and is imported from numerous places around the world. The main by-products are Pulverised Fuel/Fly Ash (PFA) (approx. 60%) and Furnace Bottom Ash (FBA) (approx. 15%). The PFA is generated from the entrainment of fine particles in the flue gas during combustion. PFA is generally a spherical particle with pozzolanic properties that has made it very common as a cement replacement. FBA is a larger, coarser particle that settles at the bottom of the combustion chamber and is more granular and angular. FBA has been used in civil engineering applications as a type of fill material. Images of PFA and FBA are shown in Figure 3. The ESB ceased burning coal at Moneypoint in 2025 but will continue to provide security of supply for Ireland's electricity system by operating as a back-up out-of-market generator of last resort for EirGrid. Moneypoint is being transformed into a renewable energy hub to contribute to the ESBs Net Zero carbon emissions strategy and utilising its deep-water port and existing infrastructure.

The ash produced at Moneypoint has traditionally been stored in the ash field (Figure 2(b)), which covers an area of approx. 25 hectares. The ash (approx. 4 million tonnes) is deposited in layers of PFA and PBA and compacted.

Here, PFA and FBA were blended with CEM I and summarised below:

- 90% CEM I + 10% PFA
- 75% CEM I + 25% PFA
- 65% CEM I + 35% PFA
- 80% CEM I + 20% FBA

(a) *(b)*

Figure 2 (a) Moneypoint power station and (b) ash field

(a) PFA *(b) FBA*

Figure 3 (a) Pulverized Fly-ash and (b) Furnace bottom ash

GGBS

Ground Granulated Blast Furnace Slag (GGBS) is a by-product from the iron and steel industry, widely used as a supplementary cementitious material (SCM) in concrete production. An estimated 500,000 tonnes of GGBS is available to the Irish market annually[13] in critical applications such as structural concrete, ready-mix and precast concrete and high-performance and specialist binders. Common practice in Ireland replaced traditional cement with 40-50% of GGBS. Up to 70% replacement has been specified but these are more likely in non-structural applications.

GGBS originates as a non-metallic residue from blast furnaces where iron ore, coke and limestone are melted. The molten slag is rapidly cooled to form a glassy granular material that is dried and finely ground into a powder with hydraulic properties analogous to Portland cement when activated with alkalis or lime. Typical fineness of GGBS is like Portland cement at around 380–550 m²/kg with higher fineness improving hydraulic reactions. GGBS is a pozzolanic binder as it reacts with calcium hydroxide to produce additional calcium silicate hydrates (C-S-H). Several standards govern the quality and use of GGBS as a cementitious material including ASTM C989[14], ASTM C595[15], BS EN 15167-1[16] and IS EN 197-1[17].

The move of the steel industry to Electric Arc Furnaces (EAF) to improve their decarbonisation goals and lower operating costs is affecting the reactivity of the resulting GGBS due to the high crystallinity and iron content. As the resulting molten slag is cooled and solidified in situ in EAF, its reactivity may be less than traditional GGBS. As EAF adoption increases, the availability of traditional GGBS is in declining. Some research is ongoing into the use of EAF slag valorisation[18,19].

[13] https://enterprise.gov.ie/en/publications/publication-files/reducing-embodied-carbon-in-cement-and-concrete-through-public-procurement-in-ireland.pdf

[14] ASTM C989-09 Standard Specification for Slag Cement for Use in Concrete and Mortars, 2010

[15] ASTM International. (2025). ASTM C595/C595M-25, Standard Specification for Blended Hydraulic Cements. ASTM International.

[16] BS EN 15167-1:2006 Ground granulated blast furnace slag for use in concrete, mortar and grout - Definitions, specifications and conformity criteria

[17] National Standards Authority of Ireland (NSAI), I.S. EN 197-1:2011 – Cement – Part 1: Composition, specifications and conformity criteria for common cements. Dublin, Ireland, 2011.

[18] Kim HS, Kim KS, Jung SS, Hwang JI, Choi JS, Sohn I. Valorization of electric arc furnace primary steelmaking slags for cement applications. Waste Manag. 2015 Jul; 41:85-93. doi: 10.1016/j.wasman.2015.03.019. Epub 2015 Apr 8. PMID: 25863765.

[19] https://www.ecocemglobal.com/powering-low-carbon-cement-unlocking-the-potential-of-electric-arc-furnace-eaf-slag/

Recycled Glass Powder

In principle, glass is 100% recyclable, and every tonne of glass re-melted saves ~580 kg of carbon dioxide emissions[20,21], as well as decreasing the energy needed to make glass and reducing reliance on virgin raw materials. Recycling rates across Europe vary. For example, 84% of glass is recycled in Ireland with 74% in the UK[22]. Waste glass cullet is commonly recycled, but its reuse in producing new glass is limited by its composition. Recycled cullet not recovered for glass container manufacturing (due to unsuitable composition, sizing, contamination, or market conditions) is often disposed of in landfill, which attracts Landfill Tax, adding to the cost of disposal. Container glass is uneconomic to decolourize, which means coloured glass is unlikely to be recycled by the glass industry, making its use as an SCM particularly attractive. The re-cycling of container glass cullet contributes to national *circular economy* aspirations, while at the same time eliminates all costs associated with landfill.

The incorporation of glass in cements is not a new idea and has been the subject of study for some time[23,24,25]. There are two important factors to consider in using glass as an SCM, due to the potential occurrence of alkali–silica reactions (ASRs) in concrete. Alkalis in concrete mixes can be a cause for concern. High alkali loads in concrete can trigger deleterious expansion if reactive silicate aggregates are present. The first factor is the alkali metal content and the second is particle size.

Alkali metals are introduced as metal carbonate flux, used to lower the melting temperature of the glass and comprise around 13% Na_2O by mass of the whole[26]. The alkali load in concrete is proportional to the binder content and the alkali level of the binder, expressed as equivalent sodium oxide content, where:

$$\%Na_2O\ equivalent = Na_2O + 0.658\%K_2O\ (by\ mass)$$

A suitable specification for recycled glass cullet suitable for "*flux/binders*" can be found in BS PAS 101[27]. Practically in cements, the alkali content of the binder is limited as a precaution against alkali silica reaction (ASR) at 0.6%. In most countries, alkalis are limited to the equivalent Na_2O content per cubic meter of concrete at 1.8 to 4.5 kg/m^3, depending on the reactivity classification of the aggregate used and on how variability in the binder alkali level is reported by the cement manufacturer. Alternatively, a 'low alkali' binder, defined as one that does not exceed 0.6% Na_2Oeq, may be used if aggregate reactivity is high or unknown.

The second consideration is the particle size of the glass. The suppression of alkali silica reaction is also addressed by fine grinding of the glass (to a few microns), as has been demonstrated elsewhere[25], and it has been found that the addition of glass powder can enhance ASR resistance if the particle size is below 300 microns[26]. This introduces another dimension to using glass powder in blended cement, that of grinding energy. To grind a material to increasingly smaller sizes, commensurate amounts of energy are required.

[20] M. Tyrer and J. Newell, "Through a glass brightly," CONCRETE, p. 4, 2025

[21] Glass, B. Glass Sector Net Zero Strategy 2050; British Glass: Sheffield, UK, 2021

[22] EPA. EPS Calls for Measures to Urgently Tackle Packaging Waste Generation. Million Tonnes, Plastics Present a Serious Challenge. Available online: https://www.epa.ie/news-releases/news-releases-2023/epa-calls-for-measures-to-urgently-tackle-packaging-waste-generation-.php#:~:text=Ireland (accessed on 30 January 2024).

[23] Dhir, R.K.; Limbachiya, M.C.; Dyer, T.D. Recycling and Reuse of Glass Cullet; Institution of Civil Engineers: London, UK, 2001; ISBN 0727748971.

[24] Chen, G.; Lee, H.; Young, K.L.; Yue, P.L.; Wong, A.; Tao, T.; Choi, K.K. Glass recycling in cement production—An innovative approach. Waste Manag. 2002, 22, 747–753.

[25] Idir, R.; Cyr, M.; Tagnit-Hamou, A. Pozzolanic properties of fine and coarse color-mixed glass cullet. Cem. Concr. Compos. 2011, 33, 19–29.

[26] Ke, G.; Li, W.; Li, R.; Li, Y.; Wang, G. Mitigation effect of waste glass powders on alkali–silica reaction (ASR) expansion in cementitious composite. Int. J. Concr. Struct. Mater. 2018, 12, 1–14.

[27] BSI—BS PAS 101; Recovered Container Glass Specification for Quality and Guidance for Good Practice in Collection. BSI: Singapore, 2003. Appendix A

This is not a linear relationship, however, but is governed by the defect density of the material to be processed. In the case of glasses, comminution to a few microns is relatively straightforward, but further reduction is increasingly energy intensive. To summarise, there seems to be no universal rule to be drawn from the literature relating to the absolute particle size of the glass or to the hydration kinetics of such glass-blended cement, and no convincing minimum particle size has been identified which will universally avoid ASR reactions. Nonetheless, the literature suggests particles below 40µm will react completely in the cement environment without detriment.

Here, recycled glass powder (RGP) was blended with ground granulated blast furnace slag and CEM II / A-L to produce a quaternary cement. The objective is to conserve cementitious slag by its partial replacement with recycled glass powder. This study examines the likely consequence of doing so by the thermodynamic modelling of both phase evolution and solution chemistry. Two formulations were included in this study

- A cement paste containing 60% CEM II/A-L combined with 34% GGBS & 6% RGP.
- A cement paste containing 40% CEM II/A-L combined with 51% GGBS & 9& RGP.
- A control sample comprising 50% GGBS and 50% CEM II/A-L without RGP was also included.

The RGP used here was supplied by Ecocem complying with BS PAS 101[28].

Calcined clays

By calcinating suitable clays to 700-900°C, can attribute cementitious properties to be considered SCMs in concrete as a cement replacement. The lower temperatures involved reduces the embodied carbon released.

The kaolinite content in the clay dictates the reactivity and its suitability as an SCM. Under 40% kaolinite content would be considered as a low-grade reactivity clay. Above 70% is considered as most suitable. Much work has been undertaken academically and practically to demonstrate the suitability of such clays as SCMs. However, studies of calcined clays in Ireland have been limited with no large-scale sustained applications of using calcined clay in concrete. It is hoped that ongoing advancements in the field will reveal the potential of using low-grade clays in structural concrete.

Dewaela *et al*[29] studied what kinds of clay deposits with different characteristics are present in the Republic of Ireland to produce roof tiles with a consistent mineralogical composition and physical behaviour. Samples were taken from multiple sites as shown in Figure 4. They found that the clay deposits in the Republic of Ireland were dominated by a combination of illite and kaolinite, which makes higher firing temperatures possible without excessive sintering, allowing the production of denser products. They concluded that no clay deposits satisfied the demands to produce roof tiles.

Banah UK[30] were successful in making a quality SCM and geopolymer precursor from calcined kaolinite rich clay from a source in Northern Ireland. The plant in Coleraine, now closed, had a production throughflow of 200,000 tonnes of calcined clay per year. BanahCEM was produced by thermally treating an aluminosilicate clay to make it reactive in an alkaline environment using lower temperatures than those required to produce cement. One tonne of BanahCEM solids produced approximately 200kg of emissions, compared to 800kg in cement. BanahCEM reported a rapid strength gain with 50% of 28-day strength achieved after nine hours, 80% after one day and 95% after seven days. Here, calcined clay (28%) taken from James Stevenson Quarries, Antrim in Co. Antrim was blended with 55% CEM I cement, 15% ground limestone and 2% gypsum.

[28] BS PAS 101:2003, Specification for recovered container glass, British Standards Institute.

[29] Dewaele, S., Ottenburgs, R., Van Oyen, P. and Viaene, W., 2003. Prospection and evaluation of clay deposits in the Republic of Ireland. Aardkundige Mededelingen (Industrial minerals: resources, characteristics and applications), 13, pp.97-106.

[30] https://hassons.com/project/banah-uk

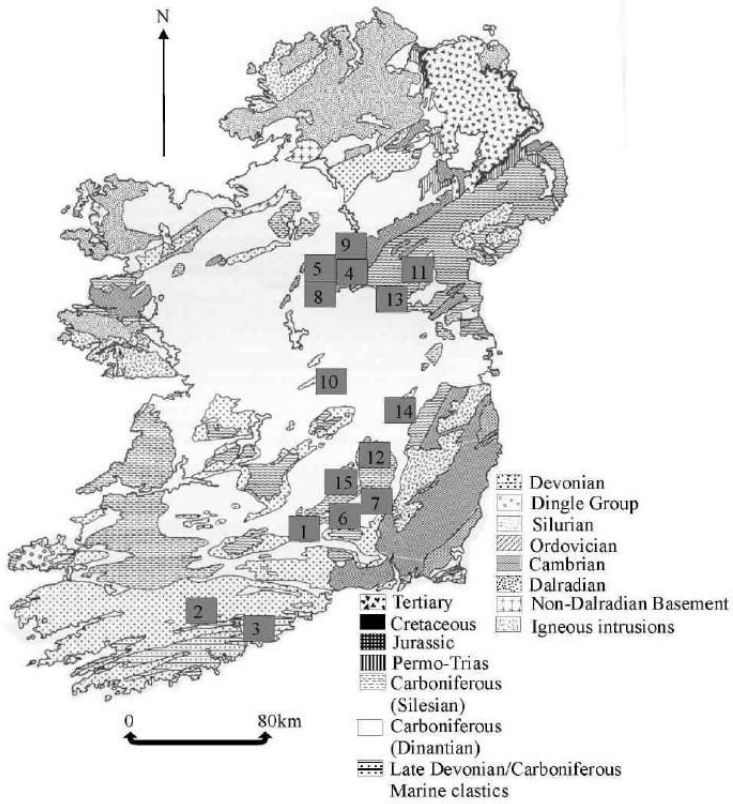

Figure 4 Samples of clays taken for assessing the suitability of roof tiles by Dewaele

Images of clay before calcination are shown in Figure 5.

Figure 5 Clay before calcination

Red mud

While an effort was made to include red mud in the list of possible cement alternatives, it was not possible to obtain samples to be included in the project. However, we feel it is important to include red mud as a possible alternative due to its use in other countries and the abundance of the material in Ireland. This is evidenced by the ongoing work by the St Loarn group to develop a new low-carbon geopolymer cement[31].

Red mud is an alkaline industrial residue generated during the Bayer process for refining alumina (Al_2O_3) from bauxite ore. Sodium hydroxide digests bauxite, dissolving alumina while leaving an iron-rich, highly

[31] https://stloarngroup.ie/

alkaline residue known as red mud. For each tonne of alumina produced, approximately 1.5 tonnes of red mud is created and has to be stockpiled with several environmental challenges including storage, causticity (pH ~10–13), heavy metal leaching and land use[32]. Red mud is typically rich in Fe_2O_3 (~30-65%), Al_2O_3 (15-25%), and SiO_2 (10-20%) which suggests it may have possible cementitious and pozzolanic properties to be used as a partial cement replacement[32]. However, low inherent pozzolanic reactivity, high iron content, specific surface area and variability in composition means raw red mud often needs processing including grinding, heat activation and blending to behave effectively as a cement replacement in combination with other supplementary materials. Previous work[33] has shown that red mud can sustain or even improve mechanical performance for cement replacement levels ranging from 5–15% by mass. Improvements in permeability and porosity, decreased chloride and sulfate ingress were also reported. Red mud has been explored in low-carbon composite binders where it participated in secondary hydration reactions with improved pore structure at optimized dosages[34] and in magnesium-based cements[35].

Aughinish Alumina

Aughinish Alumina Ltd. is located on the Shannon Estuary in County Limerick and is Europe's largest alumina refinery. The plant's primary product is alumina (aluminium oxide) which is a precursor for aluminium metal production. The bauxite ore is processed using the Bayer process which produces the alumina hydrate which is calcined to produce the final product. The waste product is bauxite residue or more commonly known as red mud (~95%) and process sand, a courser by product[36]. The red mud is treated on site to approximately 65% solids content and transported to the Bauxite Residue Disposal Area. Aughinish produces roughly 1 million tonnes of red mud and 0.15 million tonnes of process sand per year[37]. The red mud and process sand are deposited in a purpose-built Bauxite Residue Disposal Area as a dewatered solid or thickened slurry. Due to the high alkanine nature of red mud (pH > 11), its storage and management are regulated by the Environmental Protection Agency (EPA).

Geoploymer

Geopolymer concrete is produced without conventional Portland cement. Instead, it relies on the activation of cementitious binders to form a hardened concrete. These include industrial by-products rich in silica and alumina, such as fly ash, GGBS and sometimes metakaolin. When these materials are combined with alkaline activators like sodium hydroxide (NaOH) and sodium silicate (Na_2SiO_3), the process of geopolymerisation produces strong bonds that contribute to strength and durability[38]. Geopolymer concrete has gained attention for its reduced embodied CO_2 emissions compared with ordinary Portland cement concrete (OPC) with

[32] Venkatesh, C., Durga, C.S.S., Sujatha, T. et al. Microstructural evolution and mechanical property enhancement of red mud incorporated high strength concrete. Sci Rep 15, 26794 (2025). https://doi.org/10.1038/s41598-025-05596-8

[33] J. Sunkpho, P. Thangavel, D. Ranjan Kumar, W. Wipulanusat & J. Doh (2026) Sustainable use of red mud in concrete: Assessing mechanical strength, durability, and performance through machine learning models, Green Technologies and Sustainability, Volume 4, Issue 2, 100283, ISSN 2949-7361, https://doi.org/10.1016/j.grets.2025.100283.

[34] Zhao, Z., Wu, F., Dong, S., Zhang, Q., Huang, C., & Chen, L. (2024). A Low-Carbon Composite Cementitious Material Manufactured by a Combined Process of Red Mud. Buildings, 14(6), 1729. https://doi.org/10.3390/buildings14061729

[35] Wei-Ying Li, Zhi-Yuan Zhang, Jun-Bo Zhou, Preparation of building materials from Bayer red mud with magnesium cement, Construction and Building Materials, Volume 323, 2022, 126507, ISSN 0950-0618, https://doi.org/10.1016/j.conbuildmat.2022.126507.

[36] https://epawebapp.epa.ie/licences/lic_eDMS/090151b280355c49.pdf

[37] https://pure.ul.ie/en/publications/growth-of-trifolium-pratense-in-red-mud-amended-with-process-sand/

[38] V.S. Sujitha, S. Raja, Maher Ali Rusho, Simon Yishak, Advances and developments in high strength geopolymer concrete for sustainable construction – A review, Case Studies in Construction Materials, Volume 22, 2025, e04669, ISSN 2214-5095, https://doi.org/10.1016/j.cscm.2025.e04669.

reductions from 40-80% reported[39]. Geopolymer concrete microstructures are based on sodium aluminosilicate hydrate (N–A–S–H) and calcium-containing gels (C-N-A-S-H). Standard fine and coarse aggregates and admixtures are also used like conventional concrete. The literature has shown positive results in terms of compressive strengths[38] and durability[40] and suitable for aggressive environments such as marine structures, and infrastructure exposed to de-icing salts.

However, despite the positive results using geopolymer concretes, several challenges remain which include variability in supply, elevated curing temperatures needed for rapid strength gain, lack of standards and comprehensive design codes and workability issues around poor fluidity without admixtures[41]. Geopolymer concrete is a very active research area and with growing industry interest, the limitations above should be addressed in the short to medium term. Another area where research is needed is in thermodynamic modelling. The derivation of suitable C-N-A-S-H solid solution gel models is very complex with at least eight end-members now included in modern databases. This will require over one hundred discrete solid phases (DSPs) to be derived for use in PHREEQC hydration models. As a result, no thermodynamic models on the geopolymer concrete used in this study has been undertaken.

Figure 6 shows the location from where the SCMs samples were obtained. While RGP is taken in across Ireland, it was centralised in Dublin.

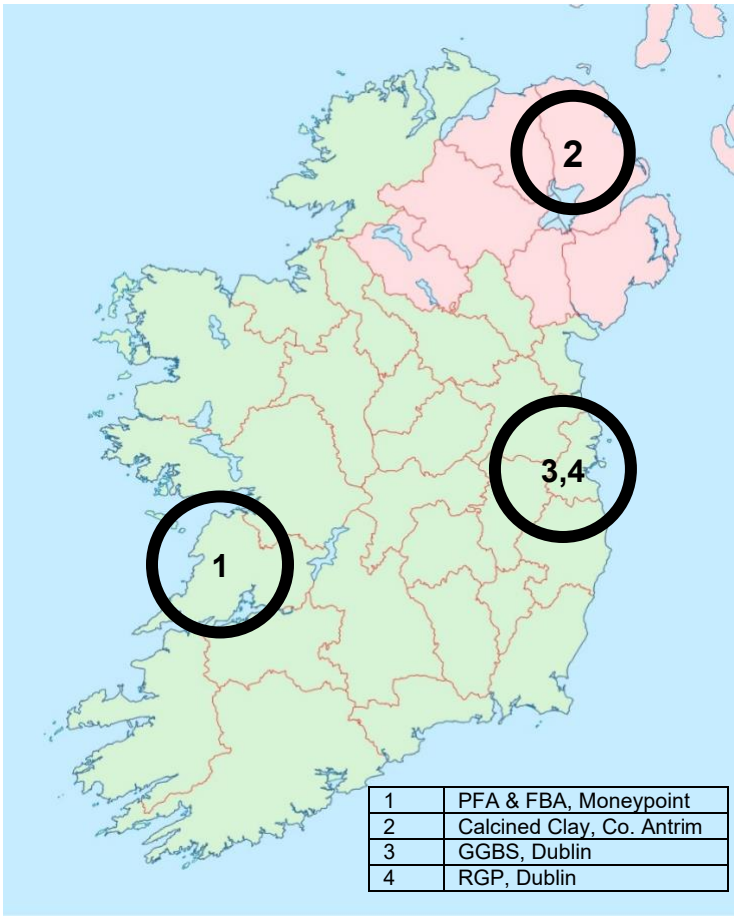

Figure 6 Sources of potential SCMs used in this project

[39] Khasawneh, M.A. Geopolymer concrete in construction projects: a review. Discov Civ Eng 2, 124 (2025). https://doi.org/10.1007/s44290-025-00281-1

[40] Alaneme, G.U., Olonade, K.A. & Esenogho, E. Eco-friendly agro-waste based geopolymer-concrete: a systematic review. Discov Mater 3, 14 (2023). https://doi.org/10.1007/s43939-023-00052-8

[41] Amer, I., Abdelkhalik, A., Mayhoub, O.A. et al. Development of Sustainable Slag-based Geopolymer Concrete Using Different Types of Chemical Admixtures. Int J Concr Struct Mater 18, 27 (2024). https://doi.org/10.1186/s40069-024-00672-1

3 SCM Characterisation

The chemical compositions of the materials were determined by X-ray fluorescence (XRF), and X-ray diffraction (XRD) was used to monitor the changing mineralogical composition over time as hydration continued.

3.1 XRF Analysis

The XRF analysis was undertaken by the Department of Geology in the University of Leicester using a Rigaku ZSX PrimusIV WD-XRF. Major elements were determined on fused glass beads prepared from ignited powders.

Table 1 Composition of the cements included in the study.

Oxide (g/100g)	CEM I	CEM II / A-L	PFA	GGBS	FBA	RGP	Calcined clay	Lime-stone	Gypsum
SiO_2	17.80	16.89	53.70	33.49	48.02	70.66	35.71	1.15	8.19
Al_2O_3	4.83	4.28	16.81	12.09	20.41	1.93	31.43	0.45	3.02
Fe_2O_3	2.82	2.56	13.46	0.88	4.67	0.40	26.23	0.26	1.08
CaO	65.60	64.64	7.41	43.58	6.46	11.91	0.72	53.75	40.25
MgO	1.88	1.66	2.08	6.73	1.35	1.18	0.40	1.04	1.30
K_2O	0.32	0.28	2.03	0.34	0.91	0.69	0.03	0.04	0.56
Na_2O	0.18	0.16	--	0.28	0.30	12.02	0.15	0.03	0.17
SO_3	2.18	1.70	1.11	1.35	0.83	0.05	0.03	0.53	38.37
P_2O_5	0.08	0.08	0.41	0.02	0.36	0.02	0.19	0.02	0.02
TiO_2	0.30	0.28	1.82	0.79	1.14	0.08	3.11	0.02	0.13
MnO	0.22	0.26	0.13	0.13	0.07	0.04	0.20	0.04	0.02
LOI	3.62	6.92	2.55	0	14.93	0.88	1.40	42.59	6.29
Density (g/cm^3)	2.95		2.24	2.49					
Blaine fineness (m^2/kg)	386	400	450	420					

Table 2 Mineralogical composition of the CEM I and PFA used (wt.%).

Phase	CEM I[a]	CEM II / A-L[a]	PFA[b]	GGBS[c]	FBA	RGP
C_3S	55.86	52.13				
C_2S	10.07	10.30				
C_3A	8.12	6.61				
C_4AF	8.24	8.35				
Lime	1.64	0.96				
Calcite	4.79	10.12				
Gypsum	4.27	4.22				
Periclase	0.96	0.96				
K_2SO_4	0.86	0.93				
Na_2SO_4	0.28	0.24				
K_2O	0.05	0.06				
Na_2O	0.15	0.13				
MgO	2.21	2.47				
SO_3	2.53	2.52				
Anhydrite				3.1		
Quartz			1.29		22.34	
Calcite			1.11		3.1	
Hematite			4.65		5.64	
Mullite			7.95		12.59	
Magnetite			3.37		9.7	
Amorphous			81.65	96.9	46.63	100

[a] CEM I composition calculated using normalisation[42]
[b] Determined using XRD Rietveld
[c] assuming 80% of amorphous phase is reactive

As shown in Table 1 most of the fly ash is SiO_2, with high levels of Al_2O_3 and Fe_2O_3. Due to the lower CaO content and alumina content between 15 and 35%, this ash can be classified as Class F, as shown in the ternary diagram (Figure 7).

[42] N. Holmes, M. Tyrer, R. P. West, A. Lowe, and D. Kelliher, Using PHREEQC to model cement hydration, Constr. Build. Mater., vol. 319, pp. 126–129, 2022, doi: https://doi.org/10.1016/j.conbuildmat.2021.126129

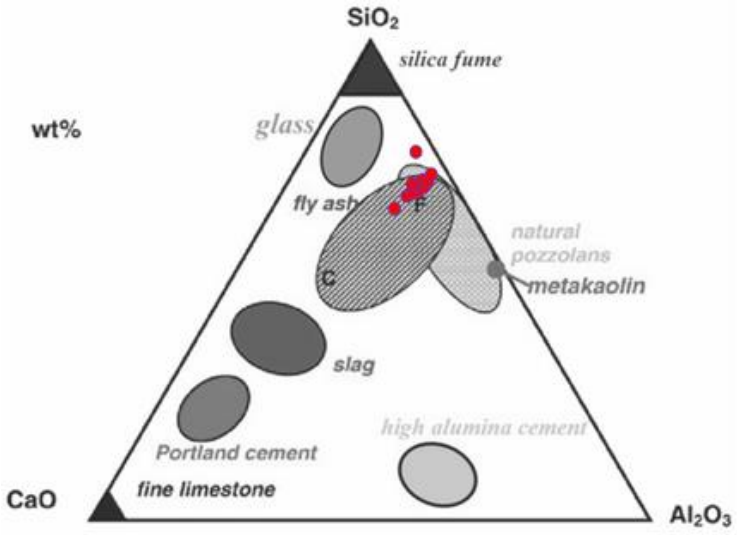

Figure 7 CaO-SiO2-Al2O3 ternary diagram.

3.2 XRD analysis

A series of cement pastes were prepared at a w/c of 0.5 and cast into 20x20x20mm cube moulds (Figure 8(a)) and cured at 20^{0}C in a water bath (Figure 8(b)). XRD was carried out at 7, 28 and 56 days, with a 20 mm cement cube being removed, powered down to 10µm and placed in the diffractometer for pattern acquisition. XRD data were collected using a Rigaku Miniflex600 spectrometer (Figure 8(c)) and scanned between 0 and 90° 2θ.

(a) 20x20x20mm cube moulds

(b) samples curing in a water bath

(c) XRD Rigaku Miniflex600 spectrometer

Figure 8 Equipment used for XRD analysis

CEM I and CEM II / A-L

Figure 9 shows the XRD pattens for hydrating CEM I and CEM II / A-L. The clinker peaks are shown at 12.1° 2θ (C_4AF), 31° 2θ (C_2S), 32.5° 2θ (mainly C_3S and C_2S) and 35° 2θ (C_3S). C_3S also overlaps with the calcite peak at 29.5° 2θ. C_2S can be difficult to identify in XRD patterns, and it appears to overlap with the C_3S peak at 32.5° 2θ, whereas C_3S is more abundant. C_3A, along with overlapping C_2S and C_3S, is observed at 32–33° 2θ.

The main hydrates, including portlandite and ettringite, along with calcite, are observed as expected. Due to the presence of approximately 4.8 g/100g of calcite in the clinker (see Table 3), permitted for CEM I cements under IS EN 197[17], monocarbonate is the most abundant AFm phase, as shown by the peak at 10.8° 2θ, which remains as hydration continues over time. Ettringite is the dominant AFt phase and is stable over time, with dominant peaks at 9, 15.8, 19 and 23° 2θ.

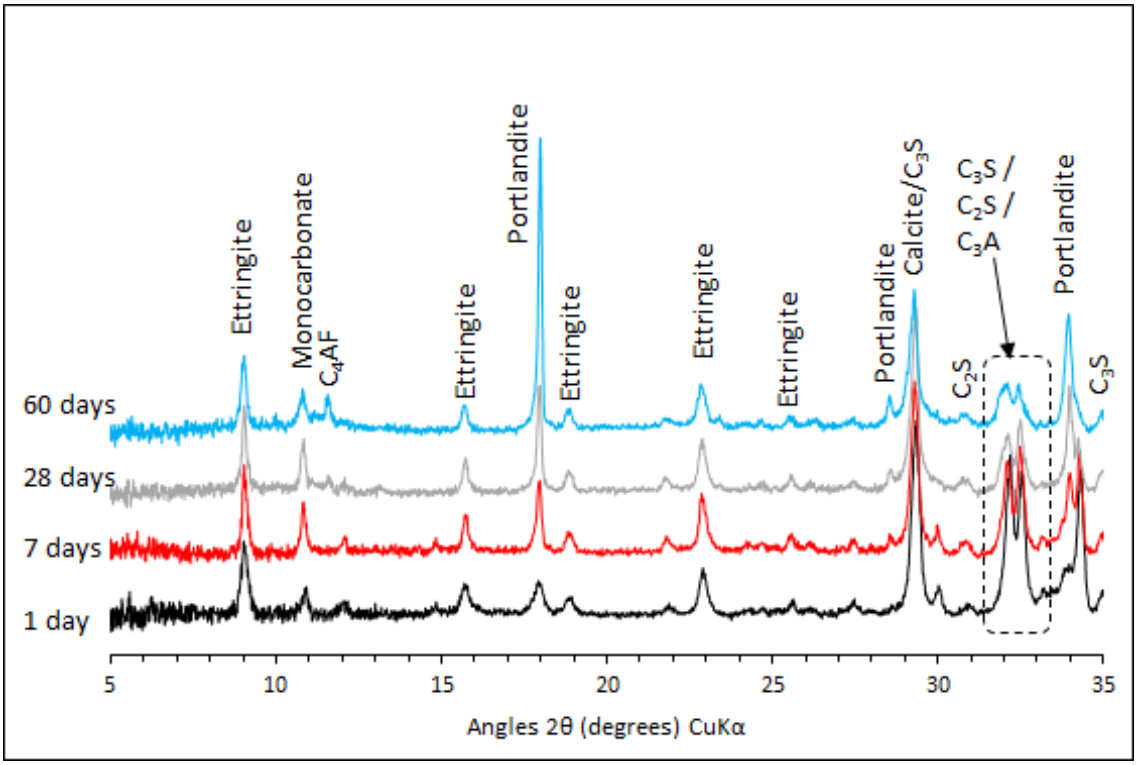

Figure 9 XRD patters from 5-35° 2θ for the CEM I

PFA

The XRD patterns of four samples taken from the ash field are shown in Figure 10. The amount of reactive silica and alumina in the ash is largely responsible for its reactivity, which has been noted previously[43]. The most abundant phases in the ash are glass (81% using a Rietveld analysis), with crystalline compounds such as quartz, calcite, hematite, mullite and magnetite, as listed in Table 2.

Particle-size distribution and SEM images of the ash taken from the site are shown in Figure 12 and Figure 13. As may be seen, the ash consists of very fine particles, with circa 99% passing a 0.1 mm sieve. This can also be seen in the SCM images taken at a 50µm resolution. Figure 13 (c & d) shows an SCM of the 20% fly ash replacement after 60 days of hydration. The images show the formation of portlandite and ettringite, as highlighted by their expected crystal formation.

[43] Alelweet, O.; Pavia, S. Potential of a low-calcium fly ash (FA) for the production of alkali-activated materials. In Proceedings of the Civil Engineering Research in Ireland, Bishopstown, Ireland, 27–28 August 2020; pp. 162–167

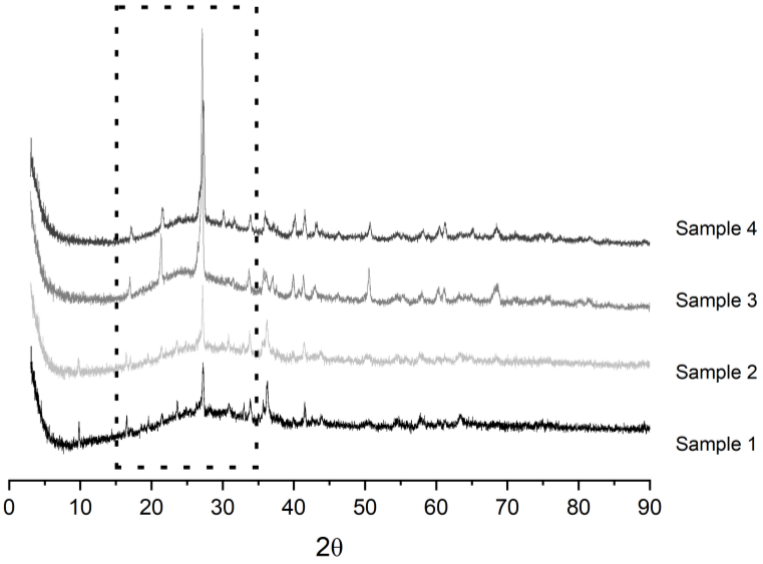

Figure 10 XRD patterns for fly ash taken from Moneypoint ash field.

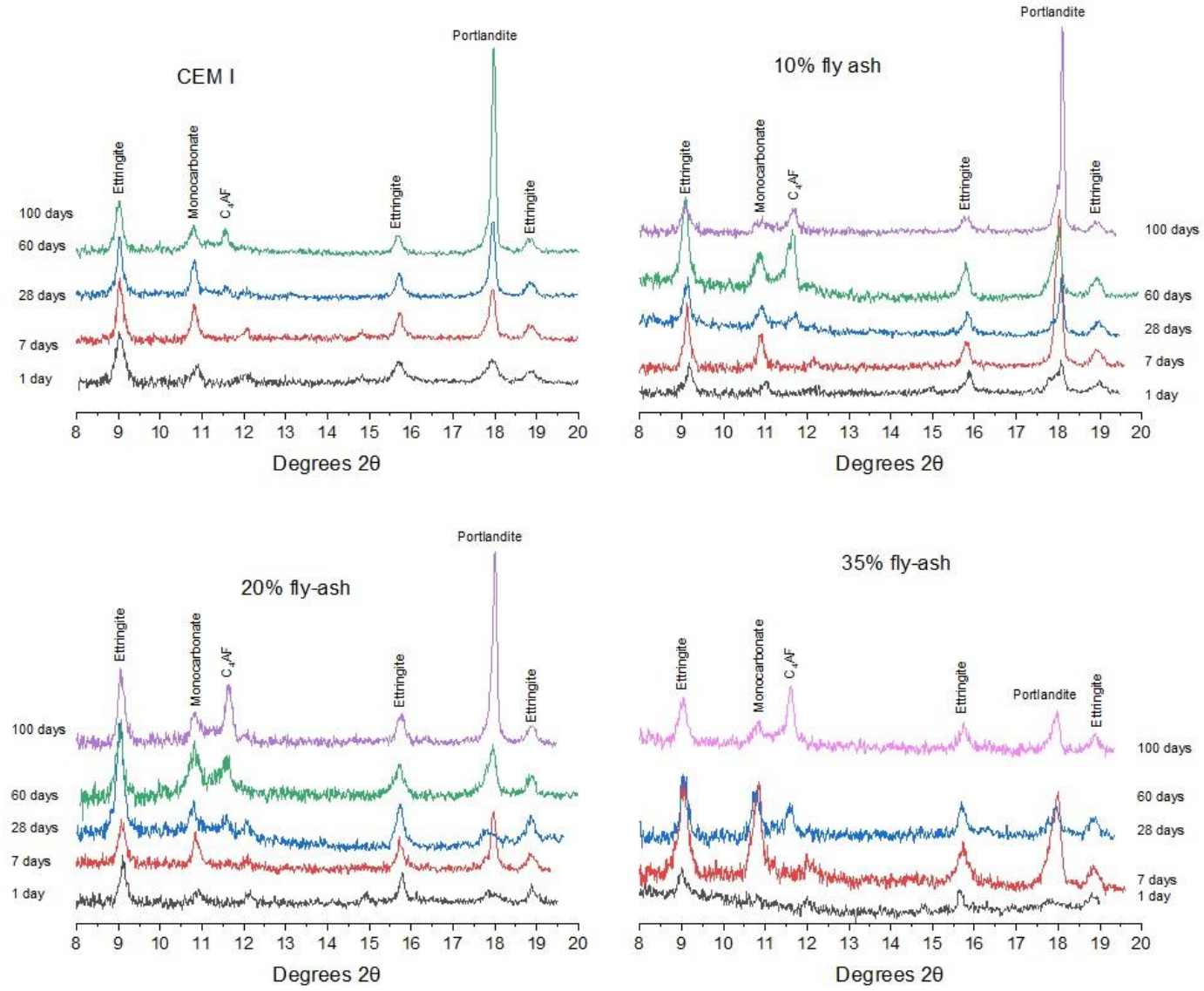

Figure 11 XRD patters of blended fly ash cements with 0, 10, 20 and 35% replacement.

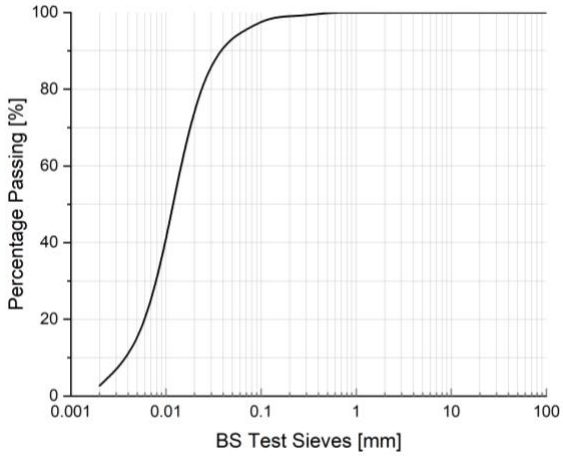

Figure 12 PFA particle size distribution using BS EN 833[44]

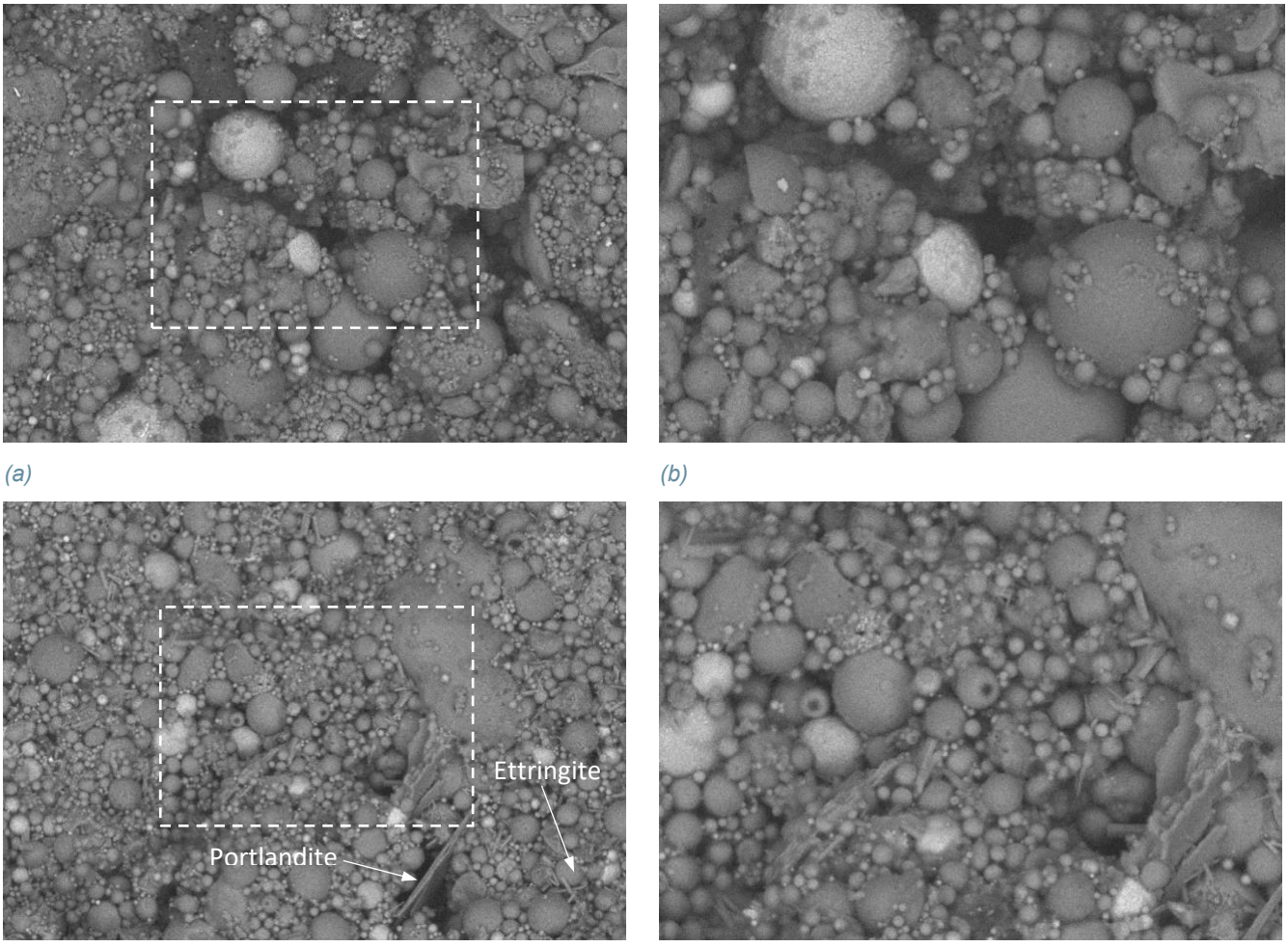

Figure 13 SEM images of unhydrated (a & b) and hydrating (c & d) cement blend with 20% fly ash after 60 days (from [45]*)*

[44] BS EN 933-1, Tests for geometrical properties of aggregates. Determination of particle size distribution. Sieving method. 2012.

[45] Shaji, N. M., Holmes, N. and Tyrer, M (2024) Early age assessment of a new course of Irish fly-ash as a cement replacement, Appl. Sci. 2024, 14. https://doi.org/10.3390/app14104128

GGBS

The XRD patterns for the blended 50-50 CEM II / A-L and GGBS cement is shown in Figure 14. The pattern shows the progressive consumption of clinker phases, activation of slag and the formation of hydration products at 7, 28, and 56 days. At 7 days of hydration, the XRD pattern is still dominated by peaks from unhydrated clinker minerals. Alite, belite and aluminate are visible at 2θ values around 32–34°, indicating incomplete hydration of the clinker. The ferrite phase is shown at 11-12^0. Portlandite is shown with characteristic reflections near 18° and 34° 2θ. Ettringite is also well observed with peaks appearing around 9°, 15–16° and 22–23° 2θ due to early sulfate reactions. A calcite peak, originating from the limestone addition in CEM II/A-L, are prominent and remain essentially unchanged with time, appearing near 29° 2θ.

By 28 days, the XRD pattern shows a somewhat reduction in the intensity of clinker phase peaks, particularly alite, indicating ongoing hydration. Belite reflections may still be present but at lower intensity. Portlandite peaks often reach a maximum or begin to decrease slightly at this stage, as calcium hydroxide is progressively consumed due to pozzolanic reactions with the GGBS and converted to C-A-S-H. Ettringite remains detectable, though its intensity may stabilise or slightly decrease depending on sulfate availability and conversion processes. Monocarbonate appears around 12° 2θ though it is often poorly crystalline and difficult to distinguish.

At 56 days, the XRD pattern is characterised by further reduction of clinker mineral peaks, with alite still detectable but less intense. Portlandite is still observed but lower than previously. Calcite peaks remain unchanged. Overall, the progressive increase in amorphous content and the reduction of portlandite and clinker phases with time are characteristic features of hydrated CEM II/A-L systems containing GGBS.

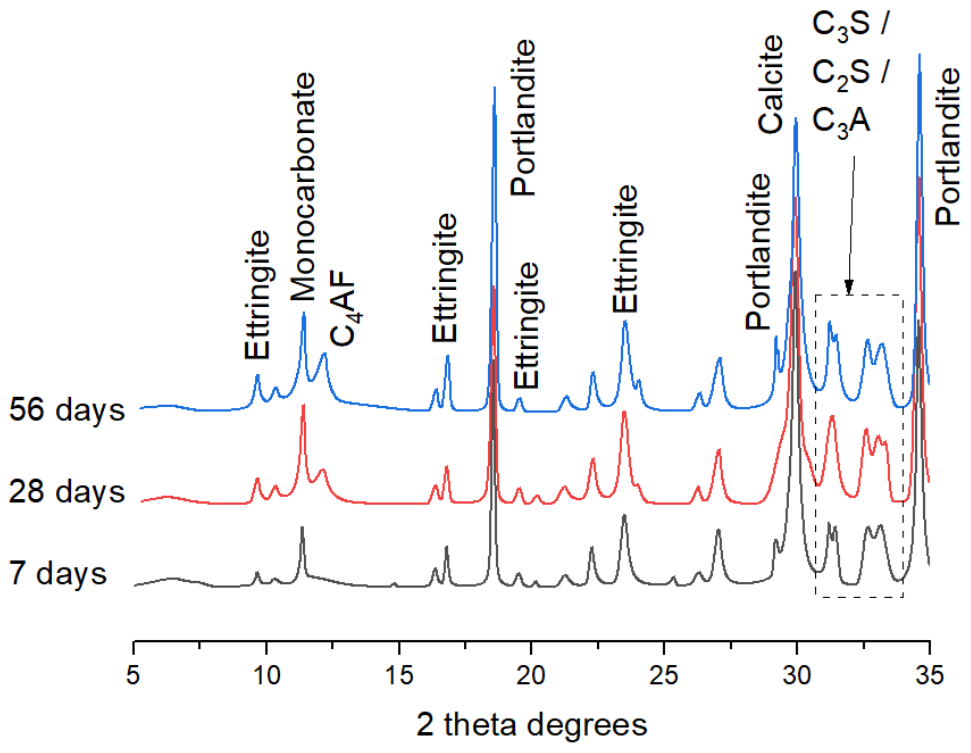

Figure 14 XRD patterns of 50-50 blended CEM II / A-L and GGBS at 7, 28 and 56 days from 5 to 35 2θ

FBA

The XRD pattern of the blended cement composed of 80% CEM I and 20% FBA is shown in Figure 15. As seen previously, at 7 days, the patterns show residual clinker phases which slowly reduce over time and they dissolve into solution. Strong patterns exist for the portlandite, ettringite and calcite phases as before. There does not appear to be any monocarbonate present but over time, the expected patterns at 11° 2θ does appear. The crystalline phases in the FBA including quartz and mullite are not clear in the XRD patterns. The broad amorphous hump between approximately 20° and 35° 2θ reflects both the glassy fraction of the FBA and early C–A-S–H formation.

As hydration continues, the clinker phases continue to dissolve and portlandite is seen to reduce, albeit marginally due to ongoing pozzolanic activity. The pozzolanic behaviour of the FBA is not expected to be as significant as PFA. Ettringite remains stable depending on sulfate availability. The FBA crystalline phases remain essentially unchanged, confirming their largely inert behaviour.

By 56 days the clinker phases peaks are significantly reduced. Portlandite is still present and often remains relatively stable with only a slight decrease, indicating limited consumption by pozzolanic reactions compared to PFA and GGBS previously. Ettringite still persists while AFm phases remain difficult to resolve due to low crystallinity.

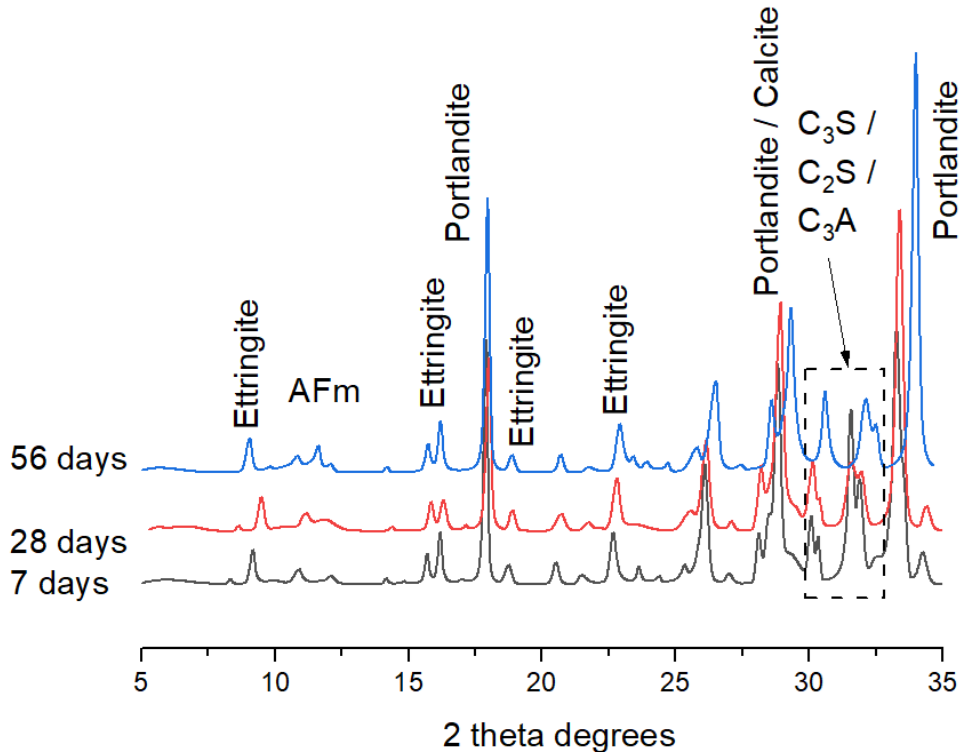

Figure 15 XRD patterns of 80-20 blended CEM I and FBA cement at 7, 28 and 56 days from 5 to 35 2θ

RGP

60% CEM II/A-L combined with 34% GGBS & 6% RGP

The XRD patterns for the 6% RGP binder are shown in Figure 16. In such a blended cement, there is significant interplay between clinker hydration, slag activation, limestone reactions and the largely amorphous nature of glass and C–A-S–H.

At 7 days, the XRD pattern is shown to be dominated by the crystalline hydration products from Portland cement, namely portlandite (18° and 34° 2θ), ongoing clinker phases hydration (12, 29–34° 2θ) and ettringite (near 9°, 16 and 23° 2θ). Calcite from the limestone component in CEM II/A-L is evident with strong consistent peak at 29° 2θ. Both GGBS and most of the RGP are largely amorphous but contribute to a broad diffuse hump between 20–35° 2θ. This is characteristic of glassy phases and poorly crystalline C–A-S–H.

At 28 days, the ongoing microstructural development is reflected by the change in intensity of portlandite peaks due to its consumption in secondary reactions with GGBS and RGP. The amorphous hump shows increased formation of C–A–S–H. Ettringite peaks persist but may appear to be decreasing in intensity as it is converted to other AFm phases including monocarboaluminate or hemicarboaluminate between 11–12° and 29–30° 2θ. Calcite peaks remain stable as limestone acts mainly as a filler and reactant for carboaluminate formation. Unhydrated clinker peaks are reducing but still detectable. Overall, the crystalline fraction shifts toward more stable AFm phases.

At 56 days, portlandite peaks are further diminished due to continued slag and glass powder reactions. The amorphous hump is showing increasing amounts of C–A–S–H gel, which remains poorly crystalline and therefore not easy to detect with sharp diffraction peaks. Ettringite is stable as sulfate remains available in the system. Calcite peaks remain strong.

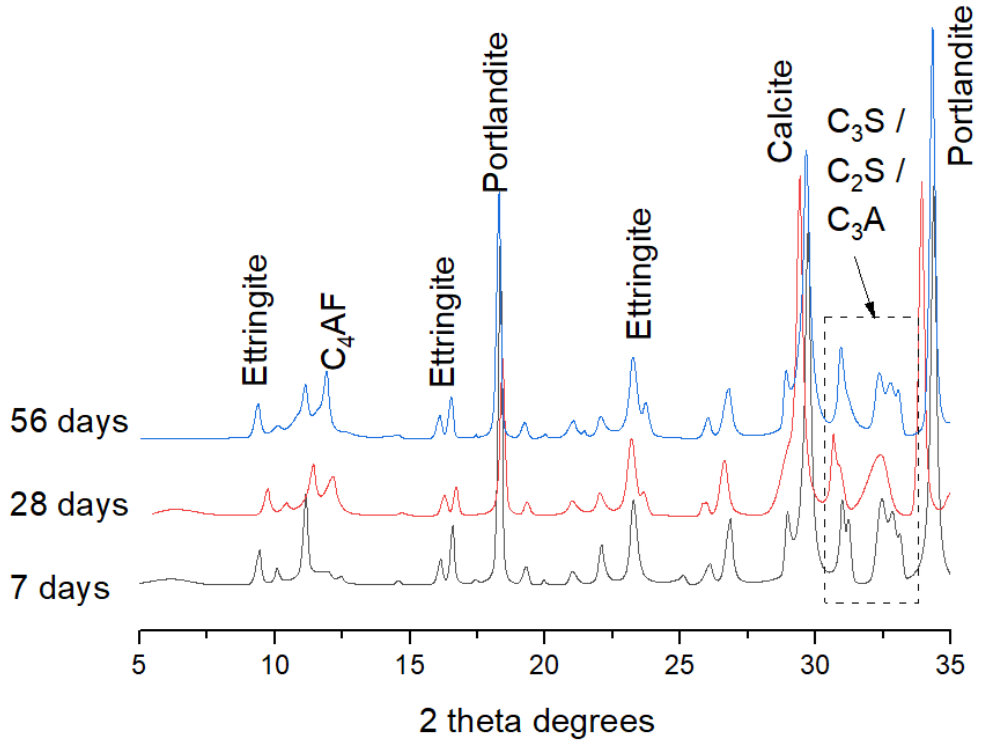

Figure 16 XRD patterns for the 60% CEM II/A-L, 34% GGBS & 6% RGP blended cement at 7, 28 and 56 days

40% CEM II/A-L combined with 51% GGBS & 9% RGP

The XRD patterns for the blended 40% CEM II/A-L, 51% GGBS and 9% recycled glass powder (RGP) binder is shown in Figure 17. Overall, the XRD patterns are close to the 6% RGP blend. The AFm patterns appear to show stronger peaks with less portlandite overall. There is some minor shifting between the patterns at 7, 28 and 56 days across the two-theta range shown. This high-GGBS, high-glass blended system exhibits relatively low portlandite intensity at all ages. The XRD evolution from 7 to 56 days reflects a transition toward a microstructure dominated by poorly crystalline C–A–S–H gel derived primarily from slag and recycled glass reactions rather than from Portland clinker hydration alone.

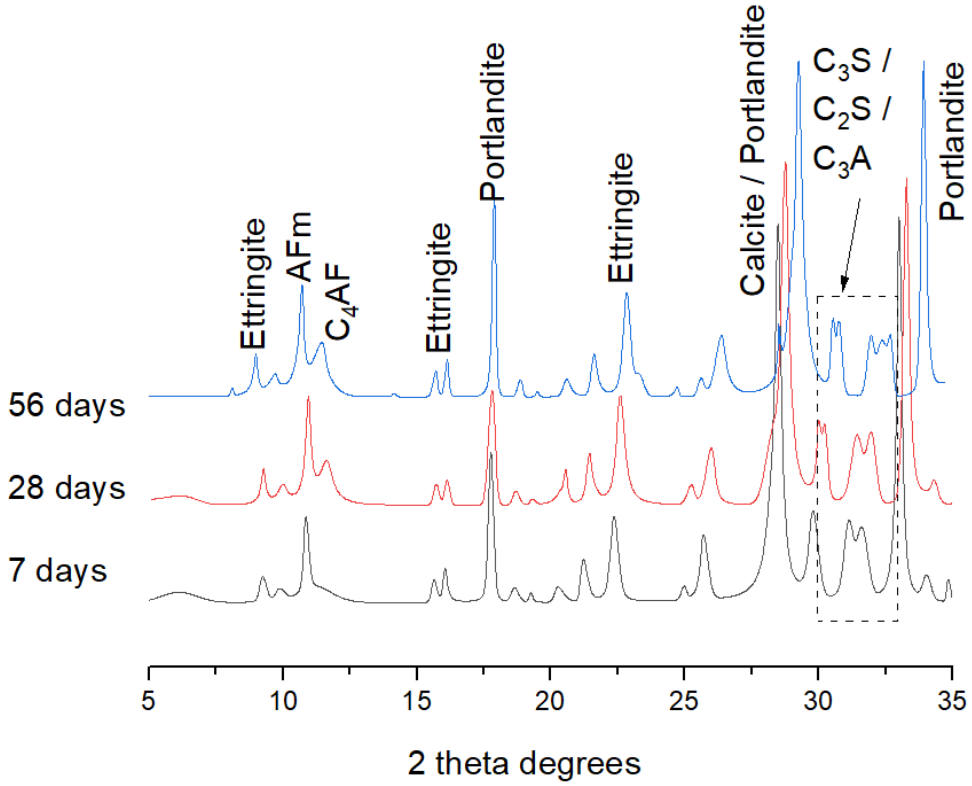

Figure 17 XRD patterns for the 40% CEM II/A-L, 51% GGBS & 9% RGP blended cement at 7, 28 and 56 days

Calcined Clay

The XRD patterns for the blended system containing 55% CEM I, 15% limestone, 2% gypsum and 28% calcined clay is shown in Figure 18. This blended cement is characteristic of a limestone–calcined clay cement (LC³-type) binder and its XRD pattern evolves significantly between 7, 28, and 56 days, reflecting clinker hydration, rapid pozzolanic reaction of calcined clay (rich in metakaolin), and the formation of carboaluminate phases due to the presence of alumina and limestone.

At 7 days, the XRD pattern shows evidence of CEM I hydration products with portlandite peaks showing at 18° and 34° 2θ. The portlandite peak at 18° 2θ has a much less intensity than has been seen before. Ettringite is also appearing due to the presence of added gypsum, with characteristic peaks at 9°, 16° and 23 2θ. Due to the additional limestone, Calcite is producing a strong peak at about 28° 2θ. Residual clinker peaks may still be visible between 12 and 30–34° 2θ. The calcined clay, largely amorphous metakaolin, contributes to a broad diffuse hump between 20° and 30° 2θ. By 7 days, the pozzolanic reaction has already begun with metakaolin reacting with portlandite, leading to early formation of AFm phases (11–12° 2θ). The amorphous content increases due to the formation of C–A–S–H gel but no sharp diffraction peaks are produced.

At 28 days, microstructural development is ongoing. Portlandite is being consumed by the pozzolanic reaction with calcined clay with increased quantities of C–A–S–H gel being produced. Ettringite peaks persist but are shown to decrease slightly as sulfate becomes depleted it partially converts to AFm phases. AFm phases are dominated by monocarbonate which is stabilised by the limestone content. The calcite peaks remain strong and relatively unchanged in intensity.

At 56 days, a mature LC³ microstructure is beginning to form. Portlandite is significantly reduced due to extensive consumption through pozzolanic reaction. AFm phases (mainly monocarbonate) are stable and clearly present. Ettringite still persists in small quantities suggesting sulfate remains in the system. The calcite peak continues to be prominent and stable.

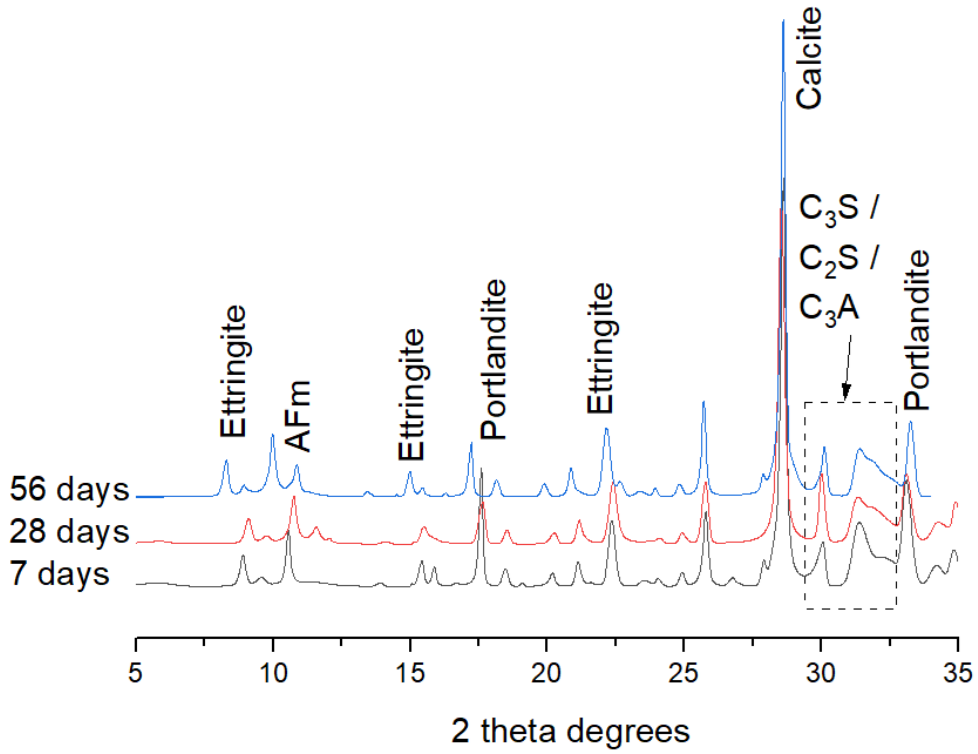

Figure 18 XRD patterns for the calcined clay binder at 7, 28 and 56 days

4 Concrete Compressive Strengths

To determine the compressive strength of the cement types included in the study, a suite of 100mm concrete cube moulds were cast and tested. The list of concrete cubes cast and their mix designs are shown in Table 3 and Table 4 below. Each mix had a w/c ratio of 0.5 with a design strength of 35Mpa at 28 days.

Table 3 Concrete mix identity and description

Mix ID	Description
1	9No. 100x100x100mm concrete with CEM I cement
2	9No. 100x100x100mm concrete with CEM II / A-L cement
3	9No. 100x100x100mm concrete with 50% CEM II / A-L cement+ 50% GGBS
4	9No. 100x100x100mm concrete with 60% CEM II / A-L + 34% GGBS + 6% RGP
5	9No. 100x100x100mm concrete with 40% CEM II / A-L + 51% GGBS + 9% RGP
6	9No. 100x100x100mm concrete with 80% CEM I cement + 20% FBA
7	9No. 100x100x100mm concrete with 55% CEM I cement + 15% Limestone + 2% Gypsum + 28% calcined clay
8	9No. 100x100x100mm concrete with 90% CEM I cement + 10% PFA
9	9No. 100x100x100mm concrete with 75% CEM I cement + 25% PFA
10	9No. 100x100x100mm concrete with 65% CEM I cement + 35% PFA

Table 4 Concrete Mix proportions

Mix ID	Mass of ingredients (kg/m^3)												
	Water	CEM I	CEM II / A-L	FA	CA		PFA	GGBS	RGP	Bot. ash	LS	Gyp.	Calcined Clay
					10mm	20mm							
1	216	432		725	491	980							
2	216		432	725	491	980							
3	216		216	725	491	980		216					
4	216		259	725	491	980		147	26				
5	216		173	725	491	980		220	39				
6	216	346		725	491	980				86			
7	216	238		725	491	980					65	9	121
8	216	389		725	491	980	43						
9	216	324		725	491	980	108						
10	216	281		725	491	980	151						

FA fine aggregate, CA course aggregate; LS Limestone

Materials

CEM I and CEM II / A-L cements complying with IS EN 197-1[17], PFA and FBA from Moneypoint, RGP donated by Ecocem, GGBS in accordance to BS EN 15167-1[16], Limestone and Gypsum from Mannok Build were used as cementitious materials. Both the fine and coarse aggregates were obtained from local sources in Ireland. The fine aggregate used was medium graded sand and the coarse aggregate was crushed limestone with a maximum size of 20mm. Before mixing, the water absorption of the aggregates was determined and the water added to the concrete was adjusted accordingly to cater for this.

Preparation of samples

The concrete was manufactured by following the procedure set-out in IS EN 206[46] using a pan mixer. For each mix in Table 1, nine 100x100x100mm concrete cubes were manufactured to determine the compressive

[46] National Standards Authority of Ireland (NSAI), I.S. EN 206:2013 – Concrete – Specification, performance, production and conformity. Dublin, Ireland, 2013.

strength at different ages for each mix. Each mix had a volume of 0.0015m^3 including 20 % for wastage. After mixing, the concrete was poured, in 50mm thick layers, into the moulds and each layer was vibrated on a vibrating table for a time until no more air bubbles were visible on the surface. Curing of the concrete was provided by placing a polythene sheet over the specimens for 24 h to trap moisture that evaporates from the surface. After demoulding the following day, the cubes were transferred to a curing tank at 20 ± 2^{0}C until they were tested.

No chemical admixtures were added to the mix design. The moisture content of the SCMs were considered negligible, as all materials were stored in a dry environment prior to mixing. No measurable moisture was detected in the GGBS, recycled powdered glass, limestone, gypsum, or calcined clays. A very small amount of moisture was observed in the FBA. However, this was minimal and did not require any adjustment to the free water content of the mix. The calcined clay mix did display some reduced workability during casting but again, no admixture was needed. The compressive strength of the concrete was determined by crushing three 100mm cubes at 7, 28 and 56 days for each mix. The test was carried out according to BS EN 12390-3[47].

Calcination of the clay

The solid clay samples obtained from James Stevenson Quarries in Co. Antrim, were initially crushed using a hammer and subsequently ground to obtain a fine powder with a particle size of less than 2mm. The crushed material was then dried in a laboratory oven at 80°C for a period of 48 hours to remove any residual moisture prior to heat treatment. Calcination was performed in a high-temperature furnace with an optimal target temperature of 750°C. The furnace temperature was increased at a controlled heating rate of 4°C/min until the target temperature was reached. At this heating rate, it took just over 3 hours to reach the 750°C target and left for 2 hours. Following calcination, the samples were allowed to cool to room temperature inside the furnace for 3 hours at which point it was further ground using a pestle and mortar and a mechanical grinder to achieve a final particle size of less than 75µm. The required quantity of the processed material was then incorporated into the concrete mix and used to cast blended concrete specimens in accordance with the calculated mix design.

Geopolymer

The PFA and GGBS used for the geopolymer concrete were the same as used for the other mixes. The activators used were sodium hydroxide (NaOH) and sodium silicate (Na_2SiO_3) with a molarity of 12 and 30 respectively. Curing of the samples was for 24hrs at 80 °C for the PFA mixes. Ambient curing was applied for the GGBS-rich mixes. The alkaline activator solution was prepared 24 hours in advance to ensure temperature stabilisation and the complete dissolving of the NaOH pellets.

Unfortunately, the compressive strength results for the geopolymer concrete were not ready in time for the report. They will be available on request from the PI if interested.

[47] BS EN 12390-3 (2009) Testing hardened concrete. Compressive strength of test specimens. British Standard Institute, London

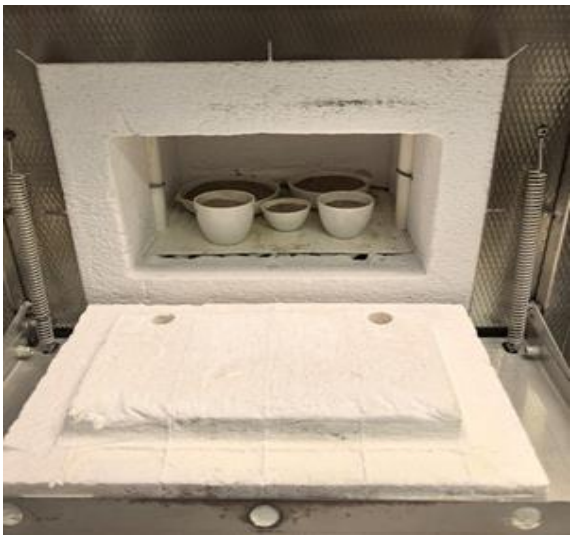

Clay in the furnace undergoing calcination *Crushed calcined clay ready for incusion in the concrete*

Figure 19 Calcined clay in the furnace and crushed, ready for inclusion in the concrete

4.1 Compressive Strength results

A summary of the compressive strength results are shown in Figure 20 and Figure 21.

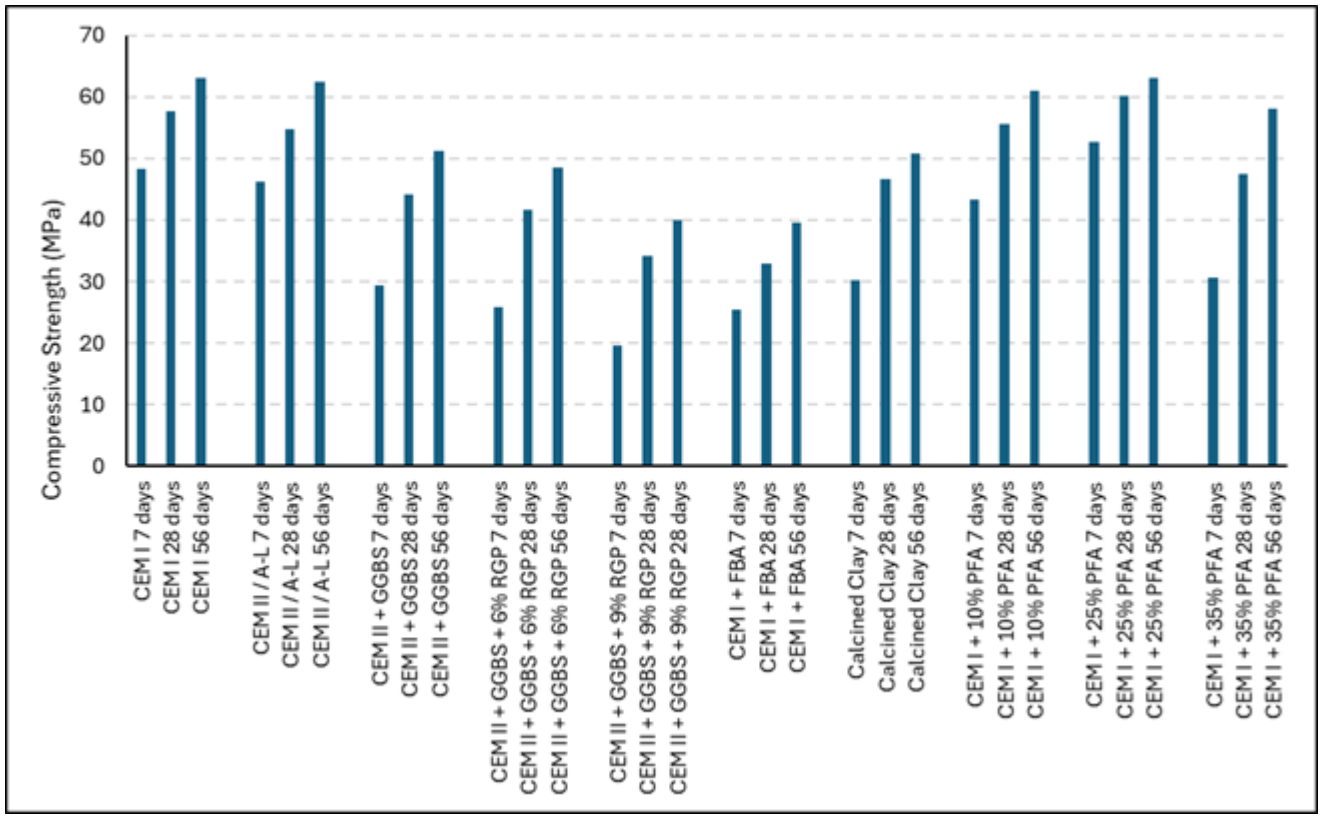

Figure 20 Full summary of compression strength results grouped by cement type

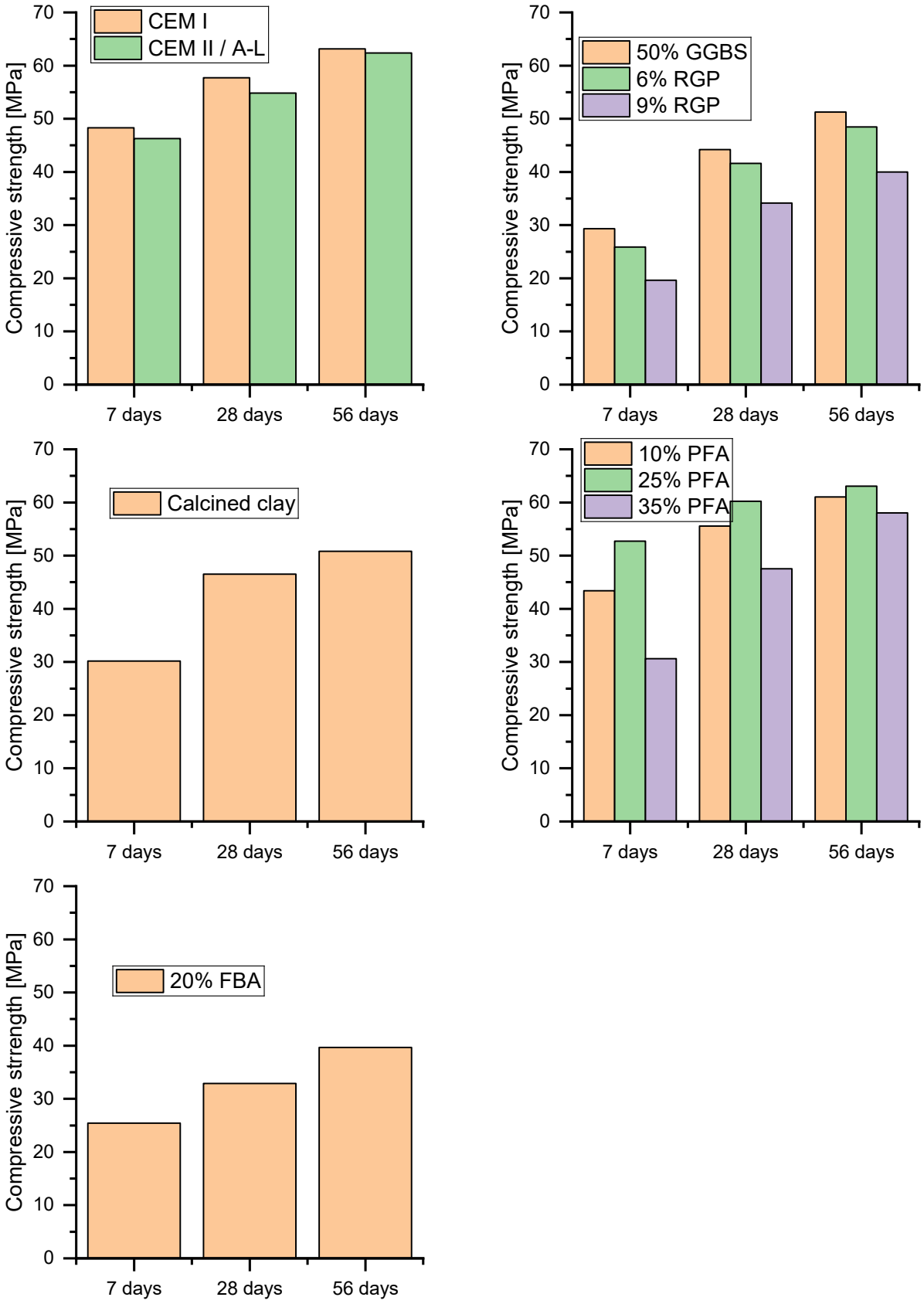

Figure 21 Compressive strength results cement by cement

Each of the concretes cast achieved the design compressive strength of 35MPa at 28 days. The highest strengths at 56 days were achieved by the CEM I, CEM II / A-L and 25% of cement replacement by PFA at over 60MPa. The use of PFA here has produced a strong concrete with reduced carbon content. While the FBA concrete did achieve the desired strength, it is the lowest overall at all ages. This is due to the lower reactivity of the FBA which is not contributing to strength development and may be even causing a loss in strength due to the reduced clinker content. Despite this, the use of FBA may have use in other construction products.

The use of RGP as a GGBS replacement does appear to have a negative effect on the strength compared to slag alone, particularly at the 9% replacement level. At 6% replacement, there is some loss in strength but it is not as much (~2-3MPa on average). Similar to the addition of PFA, the higher replacement levels do affect strength gain so it is important to find the optimum level which maximes strength while reducing overall embodied carbon.

The calcined clay concrete also shows a graduate rise in compressive strength, which has been reported previously from using this material[30]. The rise in strengths is highest from 7 to 28 days with a minor additional strength (~3MPa) at 56 days. This is especially good to see as it was the first time the PI cast calcined clay. With improvements in the calcination process and maybe improving the fineness of the clay, the strength development could be improved.

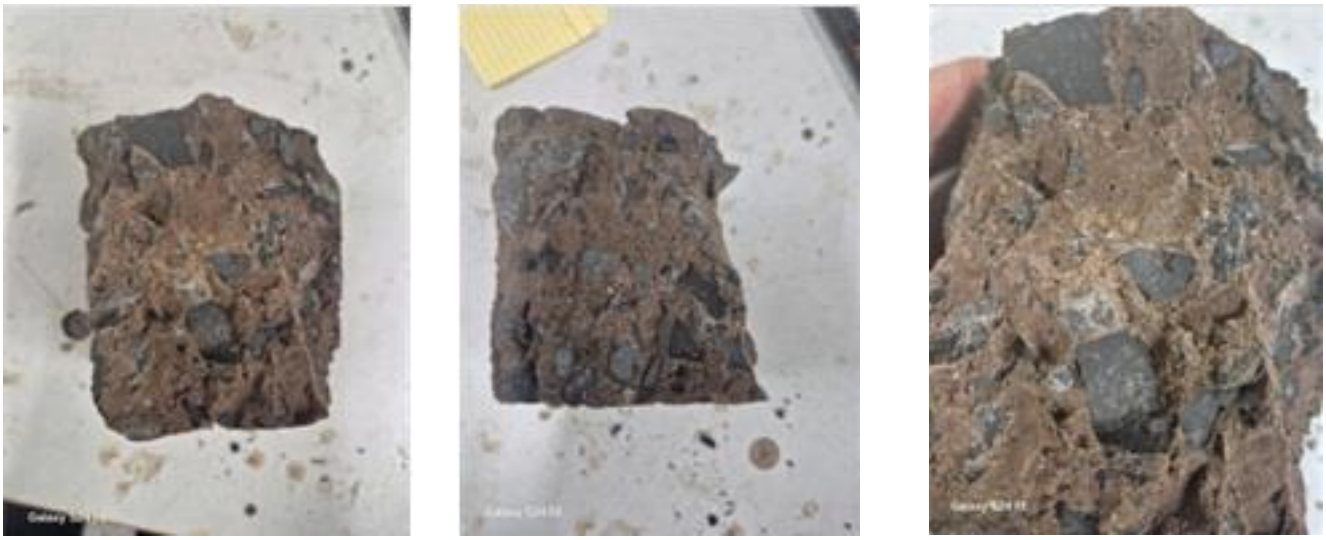

Calcined clay – 7 days | Calcined clay – 28 days | Calcined clay – 56 days

Figure 22 Images of calcined clay following compressive strength testing at 7, 28 and 56 days

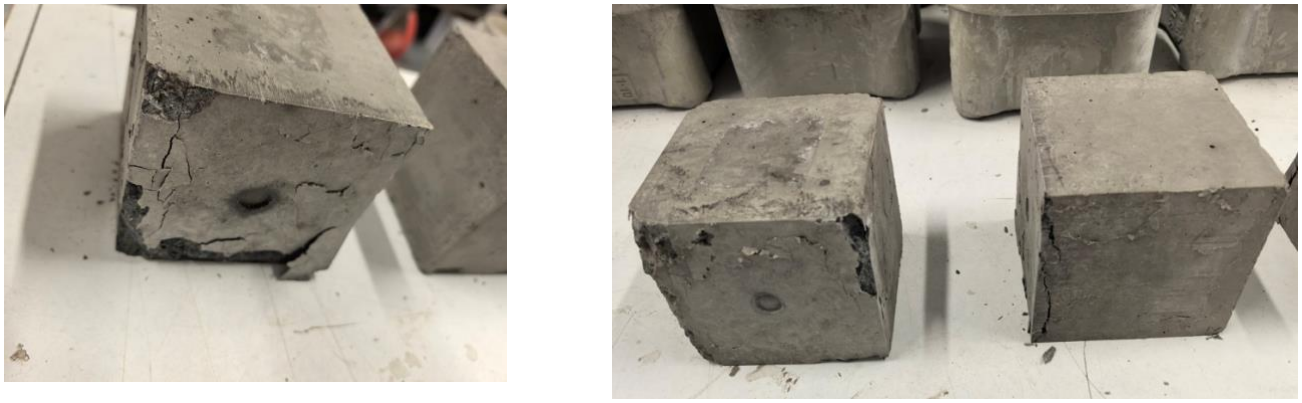

Figure 23 100mm cubes of the 50% CEM II A/L + 50% GGBS blend following compression strength testing at 28 days

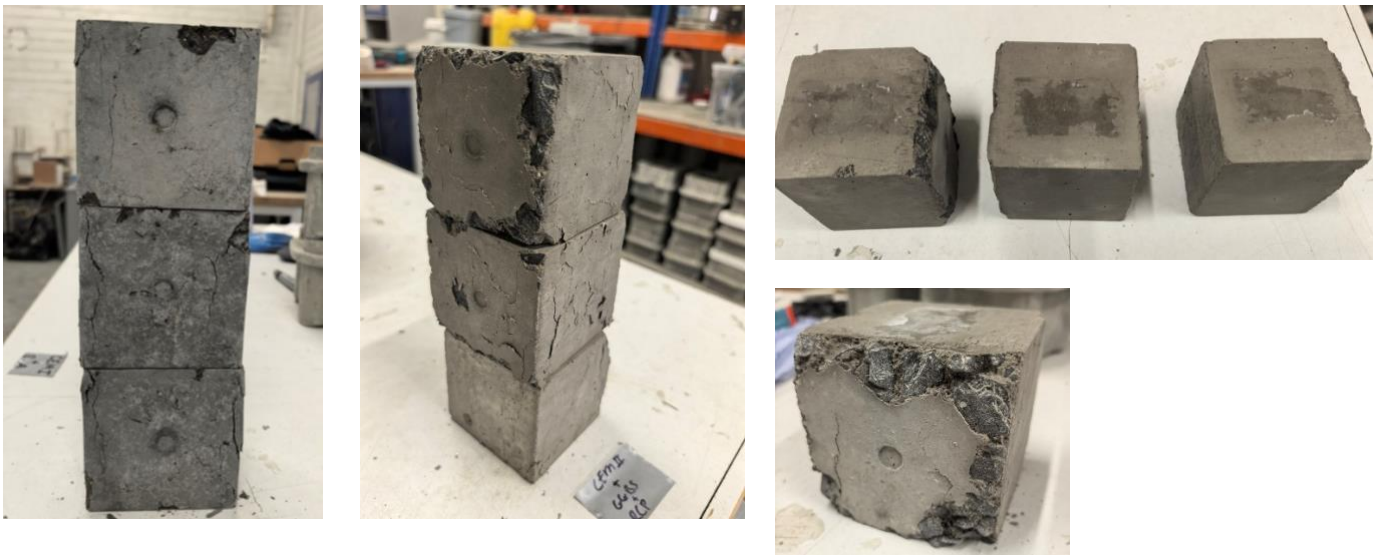

40% CEM II / A-L + 51% GGBS + 9% RPG @ 28 days

60% CEM II / A-L + 34% GGBS + 6% RPG @ 7 days

60% CEM II / A-L + 34% GGBS + 6% RPG @ 56 days

Figure 24 Selection of the cubes made with RGP following compression testing

5 Thermodynamic modelling

Thermodynamic calculations were carried out using the PHREEQC geochemical software[48,49]. PHREEQC can predict the hydration behaviour of Portland cement over time using an appropriate thermodynamic database and the molar reaction equations for the four main clinker phases alite (Ca_3SiO_5, C_3S), belite (Ca_2SiO_4, C_2S), aluminate ($Ca_3Al_2O_6$, C_3A) and aluminoferrite ($Ca_4Al_2Fe_3O_{10}$, C_4AF). PHREEQC employs the law of mass action equations to perform complex geochemical simulations, allowing for the inclusion of kinetics and rates. Here, the cemdata18 thermodynamic database[50] was used to model the predicted solid hydrates and pH over time.

Predictions of solid hydrate formation and pore solution chemistry over time using thermodynamic modelling has been shown to be a reliable method by several authors for many cement systems. To simulate hydration using thermodynamics requires descriptions of the solids and dissolved species in the system, along with data on the clinker oxide proportions, water/cement (w/c) ratio, curing temperature, relative humidity and Blaine fineness of the cement. To accurately model hydration over time, empirical rate equations are used to describe the dissolution of OPC clinker phases. Oxide components dissolved in the OPC clinker phases, the oversaturation of specific phases during the first 12 hours of hydration and the release and uptake of alkali elements (K and Na) by C-S-H are also believed to produce accurate predictions.

C-S-H in cement is amorphous and poorly crystalline with a range of molar Ca/Si ratios between 0.6 and 1.7. It displays strongly incongruent dissolution behaviour, where the release of calcium into solution is several orders of magnitude greater than that of silicon. It is, therefore, important that any cement hydration model used to predict stable phase assemblages, pH and pore chemistries over time employs a suitable C-S-H gel solubility model to accurately describe its variable composition and solubility behaviour. An example of this incongruent dissolution behaviour is given in Walker *et al*[61].

Solid solutions are homogeneous crystalline structures where one or more component can be partly or wholly substituted on specific lattice sites with moieties of equivalent charge. If the host and substituting moieties are chemically similar, the formation of an ideal solid solution is possible. However, as is often the case, differences are sufficiently large enough to cause the formation of a nonideal solid solution, which can be readily confirmed by the appearance of a miscibility gap. Solid solutions are of great importance in cement chemistry, where they can be used to describe the strongly incongruent dissolution behaviour of calcium silicate hydrate (C-S-H) gel.

If the thermodynamic properties of the unsubstituted and pure end-members are known, it is possible to calculate a series of Discrete Solid Phases (DSPs) that can be used to provide a credible thermodynamic model of cement hydration. Work by Dilnesa *et al*[51] demonstrates that DSPs can be derived for any ideal or nonideal solid solution. This approach gives full control of the input for the model with a faster follow-on analysis time and, most importantly, no loss in accuracy in the prediction of phase assemblages and pore chemistry as hydration continues.

[48] D. L. Parkhust and C. A. J. Appelo, A computer program for speciation, batch - reaction, one - dimensional transport and inverse geochemical calculations, 1999.

[49] D. J. Parkhurst and C. A. J. Appelo, Description of Input and Examples for PHREEQC Version 3 - A Computer Program for Speciation, Batch-reaction, One-dimensional Transport and Inverse Geochemical Calculations, 2013.

[50] B. Lothenbach et al., Cemdata18: A chemical thermodynamic database for hydrated Portland cements and alkali-activated materials, Cem. Concr. Res., vol. 115, pp. 472–506, 2019.

[51] Dilnesa, B.Z.; Lothenbach, B.; Renaudin, G.; Wichser, A.; Kulik, D.A. Synthesis and characterization of hydrogarnet Ca3(AlxFe1-x)2(SiO4)y(OH)4(3-y). Cem. Concr. Res. 2014, 59, 96–111

This section will describe how a full cement hydration analysis can be undertaken using PHREEQC. The cement data is applied to an Excel spreadsheet which generates the input to be copied and pasted into PHREEQC in the correct format. The cement input into the spreadsheet includes the definition of the cement composition in terms of oxide proportions (CaO, SiO_2, etc.), w/c ratio, curing temperature (°C), relative humidity (%), and Blaine fineness (m^2/kg).

OPC Normative Calculation

A normative calculation is undertaken whereby the oxide proportions are converted into molar quantities of the clinker constituents. Clinker phase proportions are determined by allocating in full or in part the oxides in the system, based on[52]. Although OPC clinker is often considered strictly anhydrous, gypsum rather than anhydrite is used here to reflect its use to prevent flash hydration of OPC. The raw clinker mass phases (g) are then normalised to represent 100 g of cement. By using 100 g of cement, the w/c ratio can be easily used to determine the water content. A w/c or w/b ratio = 0.50 for example, corresponds to 50g of water and 100g of cement/binder. Quantities of sodium and potassium sulfates are determined from $\frac{SO_3}{(K_2O + Na_2O)}$ molar ratio data shown by Taylor[53]. If this ratio is > 1.125, the molar concentration of Na_2SO_4 = moles of Na_2O·0.50 otherwise it is expressed as $\frac{SO_3}{(K_2O + Na_2O)} \cdot 0.50$. For K_2SO_4, if the $\frac{SO_3}{(K_2O + Na_2O)}$ ratio is > 1.125, its molar concentration is equal to moles of K_2O·0.9. If the ratio is < 1.125, it is expressed as $\frac{SO_3}{(K_2O + Na_2O)} \cdot 0.90$. Remaining amounts of K_2O and Na_2O are then assumed to be dissolved in the oxide clinker phases. Quantities of C_3S and C_2S are determined by a calculation of the mole fraction of C_3S, taken as $\frac{CaO}{SiO_2} - 2$.

OPC Clinker Rate Equations

The dissolution of the four main clinker phases is described by empirical rate equations proposed by Parrot and Killoh[54] and modified by Lothenbach and co-workers[55], which represent the mechanisms of nucleation and growth, diffusion and formation of a hydration shell. The controlling rate (R_t) is the lowest value from Equations 1-3 for any specified time step. A and A_0 represent the blaine fineness and reference surface area (385m^2/kg) respectively, T and T_0 are the curing temperature (K) and reference temperature of 293.15K respectively, and the fraction of clinker hydrated at each time step (α_t) is given by $\alpha_t=\alpha_t\text{-}1+\Delta_t \cdot R_{t\text{-}1}$), where time (t) is in days. An arbitrary value of $1x10^{-15}$ is chosen as the first clinker fraction hydrated. A term is included to account for relative humidity (*rh*) during curing, but which must be used with caution as R_t = 0 at a rh of 55%. The effect of w/c ratio is accounted for by using the factor (f(w/c)) as given in Equation 4 where α_t is the overall degree of hydration of the four clinker phases. This method has been used widely to model the change in weight of the clinker phases over time and in the spreadsheet using the parameters given Table 1 and Table 2.

The method uses a variable time-step and can predict the dissolution of the four phases for 1,000 days of hydration using only 47 steps.

[52] Savage, D., et al., A comparative study of the modelling of cement hydration and cement–rock laboratory experiments. Applied Geochemistry, 2011. 26: p. 1138-1152.

[53] Taylor, H.F.W., Distribution of sulfate between phases in Portland cement clinkers. Cement and Concrete Research, 1999. 29: p. 1173-1179

[54] Killoh, L.J. and D.C. Parrot, Prediction of cement hydration. Br. Ceram. Proc, 1984. 35: p. 41–53.

[55] Lothenbach, B., et al., Influence of limestone on the hydration of Portland cements. Cement and Concrete Research, 2008. 38: p. 848–860

$$R_t = \frac{K}{N}(1-\alpha_t)\left(-ln(1-\alpha_t)\right)^{(1-N)} \cdot \frac{A}{A_0} \cdot exp\left[\frac{E_a^m}{R}\left(\frac{1}{T}-\frac{1}{T_0}\right)\right] \cdot \left(\frac{RH-0.55}{0.45}\right)^4 \cdot f(\frac{w}{c}) \quad (1)$$

$$R_t = \frac{K(1-\alpha_t)^{\frac{2}{3}}}{1-(1-\alpha_t)^{\frac{1}{3}}} \cdot exp\left[\frac{E_a^m}{R}\left(\frac{1}{T}-\frac{1}{T_0}\right)\right] \cdot \left(\frac{RH-0.55}{0.45}\right)^4 \cdot f(\frac{w}{c}) \quad (2)$$

$$R_t = K(1-\alpha_t)^N \cdot exp\left[\frac{E_a^m}{R}\left(\frac{1}{T}-\frac{1}{T_0}\right)\right] \cdot \left(\frac{RH-0.55}{0.45}\right)^4 \cdot f(\frac{w}{c}) \quad (3)$$

$$f\left(\frac{w}{c}\right) = (1 + 3.333 * (H * w/c - \alpha_t))^4; \text{ for } \alpha_t > H * w/c \quad (4)$$

Table 5 Parameters used in the Parrot and Killoh degree of hydration analysis[54].

Parameter	**C_3S**	**C_2S**	**C_3A**	**C_4AF**
K^1	1.5	0.5	1.0	0.37
N^1	0.7	1.0	0.85	0.7
H	1.8	1.35	1.60	1.45
K^2	1.1	0.7	1.0	0.4
N^2	3.3	5.0	3.2	3.7
K^3	0.05	0.02	0.04	0.015
E_a^m (J/mol)	41,570	20,785	54,040	34,087

Dissolution of Oxides Dissolved in OPC Clinker

In addition to determining the clinker proportions, the spreadsheet predefines the molar amounts of the oxide components (K_2O, Na_2O, MgO & SO_3) dissolved in the OPC clinker phases (C_3S, C_2S, C_3A & C_4AF). These were defined using compositions described by Taylor[53] (Table 6). Dissolution of the oxide components is then proportional to the dissolution of the OPC clinker phases as described in the preceding section.

Table 6 Composition and percentages of oxides dissolved in cement clinker phases[53]

Clinker phase	Oxide								
	K_2O	Na_2O	MgO	SO_3		K_2O (%)	Na_2O (%)	MgO (%)	SO_3 (%)
C_3S	0.1	0.1	1.1	0.1		5.26	7.69	18.33	33.33
C_2S	0.9	0.1	0.5	0.2		47.37	7.69	8.33	67.67
C_3A	0.7	1.0	1.4	0		36.84	76.92	23.33	0
C_4AF	0.2	0.1	3.0	0		10.53	7.69	50.0	0
Total	1.9	1.3	6.0	0.3		100	100	100	100

Accessory Clinker Phases

The remaining accessory clinker phases lime, calcite, gypsum, periclase, arcanite (K_2SO_4), and thenardite (Na_2SO_4) are provided in the first time-step and allowed to reach equilibrium with the pore solution. These minerals are therefore immediately available to dissolve and contribute to the formation of hydrate solids. Due to the immediate availability of free lime and periclase for example, small amounts of portlandite and brucite are precipitated in the first time-step, along with gypsum. Table 7 describes the modelling approach for the various clinker phases in the current model where the alkalis were not included in the analysis. Gypsum is oversaturated to have a saturation index of 0.3 for the first 12 hours of hydration.

Table 7 Modelling approach for the hydration behaviour of the clinker phases

Clinker phase	Model approach
C_3S	Kinetic
C_2S	Kinetic
C_3A	Kinetic
C_4AF	Kinetic
K_2O	Kinetic (dissolved in C_3S, C_2S, C_3A & C_4AF)
Na_2O	Kinetic (dissolved in C_3S, C_2S, C_3A & C_4AF)
MgO	Kinetic (dissolved in C_3S, C_2S, C_3A & C_4AF)
SO_3	Kinetic (dissolved in C_3S & C_2S)
Na_2SO_4	Equilibrium – immediately dissolved during step 1
K_2SO_4	Equilibrium – immediately dissolved during step 1
Lime	Equilibrium – immediately dissolved during step 1
Calcite	Equilibrium – reacting instantaneous equilibrium
Gypsum	Equilibrium – reacting instantaneous equilibrium
Periclase	Equilibrium – immediately dissolved during step 1

Oversaturation

It has been reported in the literature[56] that solutions are oversaturated with respect to gypsum, portlandite, syngenite and ettringite in the first 12hrs of cement hydration. To increase the solubility of all precipitating solids (including portlandite, C-S-H, gypsum, brucite, syngenite & ettringite) in the first 12hrs, an oversaturation factor of 0.15(n) has been applied, where n is the number of number of charged species involved in the dissolution reaction (as shown in Table 8). Furthermore, as a result, gypsum is inhibited from precipitating as it would be fully depleted within this 12-hour timeframe. The oversaturation factor is used as the target saturation index in the EQUILIBRIUM PHASES keyword for the phase in the solution. In the input file, this value returns to zero after 12 hours of hydration.

Table 8 Number of charged species (n) involved in the dissolution reaction of each phase used to account for oversaturation (saturation index, S.I. = 0.15·n) during the first 12 hours of OPC hydration.

Phase	**Composition**	**Charged species**							***n***	**S.I. < 12 hrs**
		K^+	Ca^{2+}	Mg^{2+}	OH^-	$Al(OH)_4^-$	$SiO(OH)_3^-$	SO_4^{2-}		
Brucite	$Mg(OH)_2$			1	2				3	0.45
C-S-H	$(CaO)_{1.65}(SiO_2)(H_2O)_{2.1167}$		1.65		2.3		1		4.95	0.742
Ettringite	$Ca_6(Al(OH)_6)_2(SO_4)_3(H_2O)_{26}$		6		4	2		3	15	2.25
Gypsum	$CaSO_4(H_2O)_2$		1					1	2	0.30
Portlandite	$Ca(OH)_2$		1		2				3	0.45
Syngenite	$K_2Ca(SO_4)_2(H_2O)$	2	1		-			2	5	0.75

Alkalis binding to the C-S-H

The distribution of the alkali elements K and Na between the pore solution and the C-S-H is performed within the PHREEQC KINETIC and RATES data blocks. Lothenbach *et al*[57,56] used a distribution coefficient (kd, mL/g) of 0.42 for both K and Na based on C-S-H gel having a Ca:Si ratio = 1.8 following the work of Hong *et al*[58].

[56] Winnefeld, F. and B. Lothenbach, Thermodynamic modelling of the hydration of Portland Cement. Cement and Concrete Research, 2006. 36: p. 209-226

[57] Lothenbach, B., et al., Influence of limestone on the hydration of Portland cements. Cement and Concrete Research, 2008. 38: p. 848–860

[58] Hong, S.Y. and F.P. Glasser, Alkali binding in cement pastes: Part I. The C-S-H phase. Cement and Concrete Research, 1999. 29: p. 1893– 1903

Hydrogarnet Solid Solution

The variable composition of hydrogarnet in terms of possible (Al^{3+}, Fe^{3+})$_2$ and (SiO_4^{4-},$4OH^-$)$_3$ substitutions was represented as a series of DSPs based on an ideal binary solid solution between Katoite_AlSi0$_8$ ($Ca_3Al_2(SiO_4)_{0.8}(OH)_{8.8}$) and Katoite_FeSi$_{134}$ ($Ca_3Fe_2(SiO_4)_{1.34}(OH)_{6.64}$) end members. These end members were selected to avoid the potential problems in crossing the projected miscibility gap. The DSP representing the binary solid solutions are listed under the EQUILIBRIUM_PHASES data block.

Full hydration analysis

The spreadsheet defines the required input for every time step up to 1,000 days hydration as a series of 47 individual solutions. The time intervals used here allows the analysis to be undertaken in a relatively short simulation time providing an account of oversaturation for the initial 12 hours and proportional dissolution of K_2O, Na_2O, MgO and SO_3 components dissolved in the OPC clinker phases. Output from the full analysis can be given as tabular and/or graphical formats. The current output provided includes volume and mass phase assemblages, clinker dissolution and degree of hydration, pH, pore solution chemistry, Ca:Si ratios in the C-S-H system and ionic strength after each time step.

As may be seen, the greatest difference between the two cements is the calcite ($CaCO_3$) content; 4.79g and 10.12g in the CEM I and CEM II/A-L cement, respectively. As CEM I and CEM II/A-L are permitted to contain up to 5% and 14% respectively in accordance with IS EN197-1[17], these proportions are reasonable. The oxide composition, w/c ratio and curing temperature (for the CEM I cement) are input into the spreadsheet.

CEM I and CEM II A/L cement models

The C-S-H gel model for the CEM I, CEM II / A-L was taken from the JAEA database[59] with a constant Ca:Si ratio of 1.65. The data below is added into the PHREEQC module under the PHASES datablock.

CSH165

$(CaO)_{1.65}(SiO_2)(H_2O)_{2.1167}$ + 3.3 H+ = 1.65 Ca^{+2} + 1 SiO_2 + 3.7667 H_2O

log_k 29.0129

delta_h -39.446 kcal/mol

analytical_expression -7.952197E+2 -1.084834E-1 5.343236E+4 2.855904E+2 -2.605524E+6

[59] C. S. Walker et al., The JAEA thermodynamic database for reactions between groundwater, cement, clay, zeolite, and/or rock forming minerals, 2016

PFA models

The gel model used for the PFA analysis allows for the additional aluminium in the phase and is written as C-(A)-S-H. It was modelled using a number of DSPs based on the continuous solid solution between five end-members with different Ca/Si and Al/Si ratios, described by Shaji *et al*[60]. Details on how DSPs are derived can be found in Walker *et al*[61]. Holmes *et al*[62] previously demonstrated this approach for the derivation of DSPs for the CSH-3T and CSHQ end-members. The thermodynamic data for the derivation of DSP is taken from the cemdata18 database and are copied directly into the PHREEQC input file. The amorphous/glass phase of the glass was modelled using phase equations following the methodology described in Shaji *et al*[60]. The full suite of end-members and DSPs for the C-(A)-S-H phases are given in Table 9.

Table 9 End-members (in bold) and DSP for the C-A-S-H model

Phase	DSP Dissolution Reaction	log k (25°C)	Analytical Expression *		
			a	*c*	*d*
INFCA	**$(CaO)(Al_2O_3)_{0.15625}(SiO_2)_{1.1875}(H_2O)_{1.65625}$ + 1.6875 H^+ = 1 Ca^{2+} + 0.3125 AlO_2^- + 2.5 H_2O + 1.1875 SiO_2**	**8.95**	**-4.74**	**2835.08**	**1.69**
$CASH_1$	$(CaO)(Al_2O_3)_{0.125}(SiO_2)_{1.25}(H_2O)_{1.825}$ + 1.75 H^+ = 1 Ca^{2+} + 0.25 AlO_2^- + 2.7 H_2O + 1.25 SiO_2	9.51	-7.78	2940.57	3.00
$CASH_2$	$(CaO)(Al_2O_3)_{0.09375}(SiO_2)_{1.3125}(H_2O)_{1.99375}$ + 1.8125 H^+ = 1 Ca^{2+} + 0.1875 AlO_2^- + 2.9 H_2O + 1.3125 SiO_2	10.20	-10.66	3046.05	4.30
$CASH_3$	$(CaO)(Al_2O_3)_{0.0625}(SiO_2)_{1.375}(H_2O)_{2.1625}$ + 1.875 H^+ = 1 Ca^{2+} + 0.125 AlO_2^- + 3.1 H_2O + 1.375 SiO_2	10.97	-13.48	3151.54	5.61
$CASH_4$	$(CaO)(Al_2O_3)_{0.03125}(SiO_2)_{1.4375}(H_2O)_{2.33125}$ + 1.9375 H^+ = 1 Ca^{2+} + 0.0625 AlO_2^- + 3.3 H_2O + 1.4375 SiO_2	11.81	-16.22	3257.02	6.91
TobH-CNASHss	**$(CaO)\ (SiO_2)1.5(H_2O)_{2.5}$ + 2 H^+ = 1 Ca^{2+} + 3.5 H_2O + 1.5 SiO_2**	**12.80**	**-18.82**	**3362.51**	**8.22**
$CASH_5$	$(CaO)_{1.05}(Al_2O_3)_{0.15}(SiO_2)_{1.15}(H_2O)_{1.65}$ + 1.8 H^+ = 1.05 Ca^{2+} + 0.3 AlO_2^- + 2.55 H_2O + 1.15 SiO_2	10.12	-5.75	3313.21	1.92
$CASH_6$	$(CaO)_{1.05}(Al_2O_3)_{0.11875}(SiO_2)_{1.2125}(H_2O)_{1.81875}$ + 1.8625 H^+ = 1.05 Ca^{2+} + 0.2375 AlO_2^- + 2.75 H_2O + 1.2125 SiO_2	10.70	-8.76	3418.69	3.23
$CASH_7$	$(CaO)_{1.05}(Al_2O_3)_{0.0875}(SiO_2)_{1.275}(H_2O)_{1.9875}$ + 1.925 H^+ = 1.05 Ca^{2+} + 0.175 AlO_2^- + 2.95 H_2O + 1.275 SiO_2	11.42	-11.62	3524.18	4.53
$CASH_8$	$(CaO)_{1.05}(Al_2O_3)_{0.05625}(SiO_2)_{1.3375}(H_2O)_{2.15625}$ + 1.9875 H^+ = 1.05 Ca^{2+} + 0.1125 AlO_2^- + 3.15 H_2O + 1.3375 SiO_2	12.23	-14.39	3629.66	5.84
$CASH_9$	$(CaO)_{1.05}(Al_2O_3)_{0.025}(SiO_2)_{1.4}(H_2O)_{2.325}$ + 2.05 H^+ = 1.05 Ca^{2+} + 0.05 AlO_2^- + 3.35 H_2O + 1.4 SiO_2	13.20	-17.01	3735.15	7.14
$CASH_{10}$	$(CaO)_{1.1}(Al_2O_3)_{0.14375}(SiO_2)_{1.1125}(H_2O)_{1.64375}$ + 1.9125 H^+ = 1.1 Ca^{2+} + 0.2875 AlO_2^- + 2.6 H_2O + 1.1125 SiO_2	11.44	-6.61	3791.33	2.15
$CASH_{11}$	$(CaO)_{1.1}(Al_2O_3)_{0.1125}(SiO_2)_{1.175}(H_2O)_{1.8125}$ + 1.975 H^+ = 1.1 Ca^{2+} + 0.225 AlO_2^- + 2.8 H_2O + 1.175 SiO_2	12.04	-9.59	3896.81	3.46
$CASH_{12}$	$(CaO)_{1.1}(Al_2O_3)_{0.08125}(SiO_2)_{1.2375}(H_2O)_{1.98125}$ + 2.0375 H^+ = 1.1 Ca^{2+} + 0.1625 AlO_2^- + 3 H_2O + 1.2375 SiO_2	12.81	-12.41	4002.30	4.77
$CASH_{13}$	$(CaO)_{1.1}(Al_2O_3)_{0.05}(SiO_2)_{1.3}(H_2O)_{2.15}$ + 2.1 H^+ = 1.1 Ca^{2+} + 0.1 AlO_2^- + 3.2 H_2O + 1.3 SiO_2	13.74	-15.05	4107.78	6.07
$CASH_{14}$	$(CaO)_{1.15}(Al_2O_3)_{0.1375}(SiO_2)_{1.075}(H_2O)_{1.6375}$ + 2.025 H^+ = 1.15 Ca^{2+} + 0.275 AlO_2^- + 2.65 H_2O + 1.075 SiO_2	12.82	-7.40	4269.45	2.39
$CASH_{15}$	$(CaO)_{1.15}(Al_2O_3)_{0.10625}(SiO_2)_{1.1375}(H_2O)_{1.80625}$ + 2.0875 H^+ = 1.15 Ca^{2+} + 0.2125 AlO_2^- + 2.85 H_2O + 1.1375 SiO_2	13.47	-10.33	4374.94	3.69
$CASH_{16}$	$(CaO)_{1.15}(Al_2O_3)_{0.075}(SiO_2)_{1.2}(H_2O)_{1.975}$ + 2.15 H^+ = 1.15 Ca^{2+} + 0.15 AlO_2^- + 3.05 H_2O + 1.2 SiO_2	14.36	-13.03	4480.42	5.00
$CASH_{17}$	$(CaO)_{1.2}(Al_2O_3)_{0.13125}(SiO_2)_{1.0375}(H_2O)_{1.63125}$ + 2.1375 H^+ = 1.2 Ca^{2+} + 0.2625 AlO_2^- + 2.7 H_2O + 1.0375 SiO_2	14.29	-8.11	4747.58	2.62
$CASH_{18}$	$(CaO)_{1.2}(Al_2O_3)_{0.1}(SiO_2)_{1.1}(H_2O)_{1.8}$ + 2.2 H^+ = 1.2 Ca^{2+} + 0.2 AlO_2^- + 2.9 H_2O + 1.1 SiO_2	15.05	-10.93	4853.06	3.92
5CA	**$(CaO)_{1.25}(Al_2O_3)_{0.125}(SiO_2)(H_2O)_{1.625}$ + 2.25 H^+ = 1.25 Ca^{2+} + 0.25 AlO_2^- + 2.75 H_2O + 1 SiO_2**	**15.89**	**-8.68**	**5225.70**	**2.85**

[60] Shaji, N. M., Holmes, N. and Tyrer, M (2024) Derivation of fly-ash glass phase equations for use in thermodynamic models, Proceedings of the Civil Engineering Research Association in Ireland (CERI) conference, Galway, 29-30th August, pp. 109-115, Editors W. Finnegan and M. Hajdukiewicz. ISBN 978-1-3999-9618-1

[61] C. Walker, S. Sutou, C. Oda, M. Mihara, and A. Honda, Calcium silicate hydrate (C-S-H) gel solubility data and a discrete solid phase model at 25°C based on two binary non-ideal solid solutions, Cem. Concr. Res., vol. 79, pp. 1–30, 2016, https://doi.org/10.1016/j.cemconres.2015.07.006

[62] N. Holmes, C. Walker, M. Tyrer, and D. Kelliher, Deriving discrete solid phases from CSH-3T and CSHQ end-members to model cement hydration in PHREEQC, in Civil Engineering Research in Ireland (CERI) conference, 2022, pp. 28–33.

$CASH_{19}$	$(CaO)_{1.05}(Al_2O_3)_{0.025}(SiO_2)_{1.4}(H_2O)_{2.325} + 2.05\ H^+ = 1.05\ Ca^{2+} + 0.05\ AlO_2^- + 3.35\ H_2O + 1.4\ SiO_2$	13.20	-17.01	3735.15	7.14
$CASH_{20}$	$(CaO)_{1.1}(Al_2O_3)_{0.05}(SiO_2)_{1.3}(H_2O)_{2.15} + 2.1\ H^+ = 1.1\ Ca^{2+} + 0.1\ AlO_2^- + 3.2\ H_2O + 1.3\ SiO_2$	13.74	-15.05	4107.78	6.07
$CASH_{21}$	$(CaO)_{1.15}(Al_2O_3)_{0.075}(SiO_2)_{1.2}(H_2O)_{1.975} + 2.15\ H^+ = 1.15\ Ca^{2+} + 0.15\ AlO_2^- + 3.05\ H_2O + 1.2\ SiO_2$	14.36	-13.03	4480.42	5.00
$CASH_{22}$	$(CaO)_{1.2}(Al_2O_3)_{0.1}(SiO_2)_{1.1}(H_2O)_{1.8} + 2.2\ H^+ = 1.2\ Ca^{2+} + 0.2\ AlO_2^- + 2.9\ H_2O + 1.1\ SiO_2$	15.05	-10.93	4853.06	3.92
$CASH_{23}$	$(CaO)_{1.05}\ (SiO_2)_{1.45}(H_2O)_{2.5} + 2.1\ H^+ = 1.05\ Ca^{2+} + 3.55\ H_2O + 1.450000\ SiO_2$	13.71	-18.98	3734.11	8.15
$CASH_{24}$	$(CaO)_{1.1}(Al_2O_3)_{0.025}(SiO_2)_{1.35}(H_2O)_{2.325} + 2.15\ H^+ = 1.1\ Ca^{2+} + 0.05\ AlO_2^- + 3.4\ H_2O + 1.350000\ SiO_2$	14.13	-17.15	4106.75	7.07
$CASH_{25}$	$(CaO)_{1.15}(Al_2O_3)_{0.05}(SiO_2)_{1.25}(H_2O)_{2.15} + 2.2\ H^+ = 1.15\ Ca^{2+} + 0.1\ AlO_2^- + 3.25\ H_2O + 1.25\ SiO_2$	14.71	-15.16	4479.39	6.00
$CASH_{26}$	$(CaO)_{1.2}(Al_2O_3)_{0.075}(SiO_2)_{1.15}(H_2O)_{1.975} + 2.25\ H^+ = 1.2\ Ca^{2+} + 0.15\ AlO_2^- + 3.1\ H_2O + 1.15\ SiO_2$	15.37	-13.09	4852.03	4.93
$CASH_{27}$	$(CaO)_{1.25}(Al_2O_3)_{0.1}(SiO_2)_{1.05}(H_2O)_{1.8} + 2.3\ H^+ = 1.25\ Ca^{2+} + 0.2\ AlO_2^- + 2.95\ H_2O + 1.05\ SiO_2$	16.18	-10.87	5224.67	3.85
$CASH_{28}$	$(CaO)_{1.1}\ (SiO_2)_{1.4}(H_2O)_{2.5} + 2.2\ H^+ = 1.1\ Ca^{2+} + 3.6\ H_2O + 1.4\ SiO_2$	14.76	-19.00	4105.72	8.08
$CASH_{29}$	$(CaO)_{1.15}(Al_2O_3)_{0.025}(SiO_2)_{1.3}(H_2O)_{2.325} + 2.25\ H^+ = 1.15\ Ca^{2+} + 0.05\ AlO_2^- + 3.45\ H_2O + 1.3\ SiO_2$	15.22	-17.14	4478.35	7.00
$CASH_{30}$	$(CaO)_{1.2}(Al_2O_3)_{0.05}(SiO_2)_{1.2}(H_2O)_{2.15} + 2.3\ H^+ = 1.2\ Ca^{2+} + 0.1\ AlO_2^- + 3.3\ H_2O + 1.2\ SiO_2$	15.84	-15.11	4850.99	5.93
$CASH_{31}$	$(CaO)_{1.25}(Al_2O_3)_{0.075}(SiO_2)_{1.1}(H_2O)_{1.975} + 2.35\ H^+ = 1.25\ Ca^{2+} + 0.15\ AlO_2^- + 3.15\ H_2O + 1.1\ SiO_2$	16.62	-12.91	5223.63	4.86
$CASH_{32}$	$(CaO)_{1.15}(SiO_2)_{1.35}(H_2O)_{2.5} + 2.3\ H^+ = 1.15\ Ca^{2+} + 3.65\ H_2O + 1.35\ SiO_2$	15.89	-18.94	4477.32	8.01
$CASH_{33}$	$(CaO)_{1.2}(Al_2O_3)_{0.025}(SiO_2)_{1.25}(H_2O)_{2.325} + 2.35\ H_+ = 1.2\ Ca^{2+} + 0.05\ AlO_2^- + 3.5\ H_2O + 1.25\ SiO_2$	16.39	-17.03	4849.96	6.93
$CASH_{34}$	$(CaO)_{1.25}(Al_2O_3)_{0.05}(SiO_2)_{1.15}(H_2O)_{2.15} + 2.4\ H^+ = 1.25\ Ca^{2+} + 0.1\ AlO_2^- + 3.35\ H_2O + 1.15\ SiO_2$	17.13	-14.89	5222.60	5.86
$CASH_{35}$	$(CaO)_{1.2}\ (SiO_2)_{1.3}(H_2O)_{2.5} + 2.4\ H_+ = 1.2\ Ca^{2+} + 3.7\ H_2O + 1.3\ SiO_2$	17.10	-18.81	4848.92	7.94
$CASH_{36}$	$(CaO)_{1.25}(Al_2O_3)_{0.025}(SiO_2)_{1.2}(H_2O)_{2.325} + 2.45\ H^+ = 1.25\ Ca^{2+} + 0.05\ AlO_2^- + 3.55\ H_2O + 1.2\ SiO_2$	17.72	-16.78	5221.56	6.87
T5C-CNASHss	**$(CaO)_{1.25}\ (SiO_2)_{1.25}(H_2O)_{2.5} + 2.5\ H^+ = 1.25\ Ca^{2+} + 3.75\ H_2O + 1.25\ SiO_2$**	**18.45**	**-18.53**	**5220.53**	**7.87**
$CASH_{37}$	$(CaO)_{1.25}(Al_2O_3)_{0.1}(SiO_2)_{1.05}(H_2O)_{1.8} + 2.3\ H^+ = 1.25\ Ca^{2+} + 0.2\ AlO_2^- + 2.95\ H_2O + 1.05\ SiO_2$	16.18	-10.87	5224.67	3.85
$CASH_{38}$	$(CaO)_{1.25}(Al_2O_3)_{0.075}(SiO_2)_{1.1}(H_2O)_{1.975} + 2.35\ H_+ = 1.25\ Ca^{2+} + 0.15\ AlO_2^- + 3.15\ H_2O + 1.1\ SiO_2$	16.62	-12.91	5223.63	4.86
$CASH_{39}$	$(CaO)_{1.25}(Al_2O_3)_{0.05}(SiO_2)_{1.15}(H_2O)_{2.15} + 2.4\ H_+ = 1.25\ Ca^{2+} + 0.1\ AlO_2^- + 3.35\ H_2O + 1.15\ SiO_2$	17.13	-14.89	5222.60	5.86
$CASH_{40}$	$(CaO)_{1.25}(Al_2O_3)_{0.025}(SiO_2)_{1.2}(H_2O)_{2.325} + 2.45\ H^+ = 1.25\ Ca^{2+} + 0.05\ AlO_2^- + 3.55\ H_2O + 1.2\ SiO_2$	17.72	-16.78	5221.56	6.87
$CASH_{41}$	$(CaO)_{1.3}(Al_2O_3)_{0.1}(SiO_2)(H_2O)_{1.8} + 2.4\ H_+ = 1.3\ Ca^{2+} + 0.2\ AlO_2^- + 3\ H_2O + 1\ SiO_2$	17.61	-10.81	5684.01	3.78
$CASH_{42}$	$(CaO)_{1.3}(Al_2O_3)_{0.075}(SiO_2)_{1.05}(H_2O)_{1.975} + 2.45\ H^+ = 1.3\ Ca^{2+} + 0.15\ AlO_2^- + 3.2\ H_2O + 1.05\ SiO_2$	17.92	-12.98	5682.98	4.79
$CASH_{43}$	$(CaO)_{1.3}(Al_2O_3)_{0.05}(SiO_2)_{1.1}(H_2O)_{2.15} + 2.5\ H^+ = 1.3\ Ca^{2+} + 0.1\ AlO_2^- + 3.4\ H_2O + 1.1\ SiO_2$	18.39	-15.00	5681.94	5.79
$CASH_{44}$	$(CaO)_{1.3}(Al_2O_3)_{0.025}(SiO_2)_{1.15}(H_2O)_{2.325} + 2.55\ H^+ = 1.3\ Ca^{2+} + 0.05\ AlO_2^- + 3.6\ H_2O + 1.15\ SiO_2$	18.95	-16.92	5680.91	6.80
$CASH_{45}$	$(CaO)_{1.3}\ (SiO_2)_{1.2}(H_2O)_{2.5} + 2.6\ H^+ = 1.3\ Ca^{2+} + 3.8\ H_2O + 1.2\ SiO_2$	19.65	-18.70	5679.87	7.80
$CASH_{46}$	$(CaO)_{1.35}(Al_2O_3)_{0.075}(SiO_2)(H_2O)_{1.975} + 2.55\ H^+ = 1.35\ Ca^{2+} + 0.15\ AlO_2^- + 3.25\ H_2O + 1\ SiO_2$	19.47	-12.80	6142.32	4.72
$CASH_{47}$	$(CaO)_{1.35}(Al_2O_3)_{0.05}(SiO_2)_{1.05}(H_2O)_{2.15} + 2.6\ H^+ = 1.35\ Ca^{2+} + 0.1\ AlO_2^- + 3.45\ H_2O + 1.05\ SiO_2$	19.81	-14.94	6141.28	5.72
$CASH_{48}$	$(CaO)_{1.35}(Al_2O_3)_{0.025}(SiO_2)_{1.1}(H_2O)_{2.325} + 2.65\ H^+ = 1.35\ Ca^{2+} + 0.05\ AlO_2^- + 3.65\ H_2O + 1.1\ SiO_2$	20.32	-16.91	6140.25	6.73
$CASH_{49}$	$(CaO)_{1.35}\ (SiO_2)_{1.15}(H_2O)_{2.5} + 2.7\ H^+ = 1.35\ Ca^{2+} + 3.85\ H_2O + 1.15\ SiO_2$	21.00	-18.71	6139.21	7.73
$CASH_{50}$	$(CaO)_{1.4}(Al_2O_3)_{0.05}(SiO_2)(H_2O)_{2.15} + 2.7\ H^+ = 1.4\ Ca^{2+} + 0.1\ AlO_2^- + 3.5\ H_2O + 1\ SiO_2$	21.40	-14.72	6600.63	5.65
$CASH_{51}$	$(CaO)_{1.4}(Al_2O_3)_{0.025}(SiO_2)_{1.05}(H_2O)_{2.325} + 2.75\ H^+ = 1.4\ Ca^{2+} + 0.05\ AlO_2^- + 3.7\ H_2O + 1.05\ SiO_2$	21.79	-16.81	6599.59	6.66
$CASH_{52}$	$(CaO)_{1.4}\ (SiO_2)_{1.1}(H_2O)_{2.5} + 2.8\ H^+ = 1.4\ Ca^{2+} + 3.9\ H_2O + 1.1\ SiO_2$	22.43	-18.66	6598.56	7.66
$CASH_{53}$	$(CaO)_{1.45}(Al_2O_3)_{0.025}(SiO_2)_1(H_2O)_{2.325} + 2.85\ H^+ = 1.45\ Ca^{2+} + 0.05\ AlO_2^- + 3.75\ H_2O + 1\ SiO_2$	23.41	-16.56	7058.93	6.59
$CASH_{54}$	$(CaO)_{1.45}\ (SiO_2)_{1.05}(H_2O)_{2.5} + 2.9\ H_+ = 1.45\ Ca^{2+} + 3.95\ H_2O + 1.05\ SiO_2$	23.92	-18.53	7057.90	7.59
T2C-CNASHss	**$(CaO)_{1.5}\ (SiO_2)_1(H_2O)_{2.5} + 3\ H_+ = 1.5\ Ca^{2+} + 4\ H_2O + 1\ SiO_2$**	**25.57**	**-18.25**	**7517.24**	**7.52**

* Analytical expression is used in PHREEQC to describe the variation of log K with temperature according to $\log K = a + b \cdot T + c/T + d \cdot \log(T) + e/T^2$, where $b = e = 0$ and T is absolute temperature (K).

Using the oxide proportions and phase compositions, the derived phase equations used in the thermodynamic calculations to account for the amorphous phase in the 10, 25 and 35% fly ash cement replacement are given in Table 10. These are added to the PHREEQC input file to represent the behaviour of the amorphous phases most accurately, rather than adding molar concentrations of the oxides found in the glass. In terms of kinetics, while the Parrot and Killoh methodology described above was originally developed for OPC/plain cement, it is assumed that it is still applicable for the CEM II / A-L, but this is an area where research is needed. The degree of reaction (DOR) of the PFA is slower than cement, so Equation 5 was taken from the literature[63] where α_{FA} is the degree of PFA hydration and t is time in days.

$$\alpha_{FA} = -15 + 10\ ln(t + 4.5) \quad (5)$$

Table 10 FA amorphous/glass phase equations

10% FA	$(SiO_2)_{9.219}(Al_2O_3)_{1.6537}(Fe_2O_3)_{0.8299}(CaO)_{1.3605}(MgO)_{0.5359}(K_2O)_{0.2238}(Na_2O)_{0.0002}(H_2O)_{1.4416}$ = + 9.219 SiO_2 + 3.3074 AlO_2^- + 1.6598 FeO_2^- + 1.3605 Ca^{+2} + 0.5359 Mg^{+2} + 0.4476 K^+ + 0.0004 Na^+ + 0.7264 H^+ + 1.0784 H_2O
25% FA	$(SiO_2)_{9.3805}(Al_2O_3)_{1.61}(Fe_2O_3)_{0.783}(CaO)_{1.3805}(MgO)_{0.5507}(K_2O)_{0.23}(Na_2O)_{0.0002}(H_2O)_{1.4382}$ = + 9.3805 SiO_2 + 3.22 AlO_2^- + 1.566 FeO_2^- + 1.3805 Ca^{+2} + 0.5507 Mg^{+2} + 0.46 K^+ + 0.0004 Na^+ + 0.4632 H^+ + 1.2066 H_2O
35% FA	$(SiO_2)_{9.4364}(Al_2O_3)_{1.5949}(Fe_2O_3)_{0.7667}(CaO)_{1.3874}(MgO)_{0.5559}(K_2O)_{0.2321}(Na_2O)_{0.0002}(H_2O)_{1.437}$ = + 9.4364 SiO_2 + 3.1898 AlO_2^- + 1.5334 FeO_2^- + 1.3874 Ca^{+2} + 0.5559 Mg^{+2} + 0.4642 K^+ + 0.0004 Na^+ + 0.372 H^+ + 1.251 H_2O

FBA models

The C-(A)-S-H gel model was used to model the CEM I + 20% FBA binder. Table 11 shows the derived thermodynamic equation to represent the glass phase of the FBA at the 20% replacement levels using the oxide proportions and phase compositions in Table 2. As the amorous phase of the FBA as is approximately half of the PFA, the percentage of reactive ash was set at 50%. The degree of reaction (DOR) used for the PFA (Equation 5) was also used for the FBA.

Table 11 FBA amorphous/glass phase equation for 20% replacement

20% BA	$(SiO_2)_{9.0657}(Al_2O_3)_{1.6518}(Fe_2O_3)_{0.7729}(CaO)_{1.4138}(MgO)_{0.5793}(SO_3)_{0.1556}(K_2O)_{0.2419}(Na_2O)_{0.0002}(H_2O)_{1.4191}$ = + 9.0657 SiO_2 + 3.3036 AlO_2^- + 1.5458 FeO_2^- + 1.4138 Ca^{+2} + 0.5793 Mg^{+2} + 0.1556 SO_4^{-2} + 0.4838 K^+ + 0.0004 Na^+ + 0.6902 H^+ + 1.074 H_2O

GGBS models

The C-(A)-S-H gel model was used to model the CEM II / A-L + 50% GGBS binder. Table 12 shows the derived thermodynamic equation to represent the glass phase of the GGBS at the 50% replacement levels using the oxide proportions and phase compositions in Table 1 and Table 2.

[63] De Weerdt, K.; Haha, M.B.; Le Saout, G.; Kjellsen, K.O.; Justnes, H.; Lothenbach, B. Hydration mechanisms of ternary Portland cements containing limestone powder and fly ash. Cem. Concr. Res. 2011, 41, 279–291. https://doi.org/10.1016/J.CEMCONRES.2010.11.014.

Table 12 GGBS amorphous/glass phase equation for 50% replacement

50% GGBS	$(SiO_2)_{5.2068}(Al_2O_3)_{1.3748}(Fe_2O_3)_{0.0184}(CaO)_{7.4919}(MgO)_{1.5121}(SO_3)_{0.265}(K_2O)_{0.0302}(Na_2O)_{0.0377}(H_2O)_{2.0298}$ = + 5.2068 SiO_2 + 2.7496 AlO_2^- + 0.0368 FeO_2^- + 7.4919 Ca^{+2} + 1.5121 Mg^{+2} + 0.265 SO_4^{-2} + 0.0604 K^+ + 0.0754 Na^+ - 14.8274 H^+ + 9.4435 H_2O

The degree of reaction (DOR) of the slag is slower than cement, so an empirical non-linear regression equation, employing four-parameter logistic (4PL) as suggested by Kulik *et al*[64], using Equation 6 where b is taken as 0.7, c is 85.1, d = 60 and g = 1. The DOR and change in volume for a 51g GGBS and 9g RGP blend is shown in Figure 25.

$$DOR(\%) = d + \frac{(a-d)}{1+\left(\frac{t}{c}\right)^b} \quad (6)$$

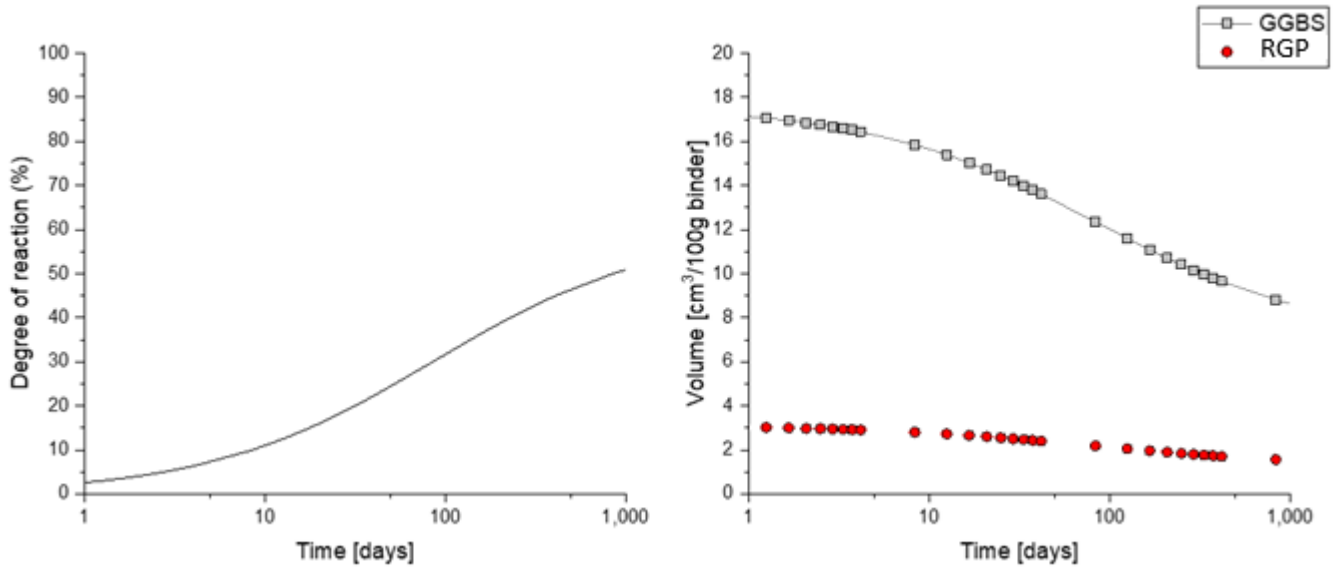

Figure 25 Left:- Degree of reaction and Right - dissolution of GGBS and RGP.

RGP models

The C-(A)-S-H gel model was used for the RCG blends. The thermodynamic input for the slag and glass powder was provided through phase equations derived from their oxide content. This method was developed by Shaji *et al*[60] to describe the glass phase of PFA in addition to the other crystalline phases. This provides a comprehensive way to include the glass phase, which will provide accurate predictions of phase assemblages, pore solution chemistry and pH. For the slag and recycled glass powder used here, it was assumed they constitute 100% amorphous glass with no crystalline phases with a 50:50 split between active and inactive glass. The reaction stoichiometries shown are based on a 1 kg = 1 mole stoichiometry, which makes it convenient to add into the required molar quantities of the PHREEQC input file. The thermodynamic phase equations for the slag and recycled glass powder used in the analysis are provided in Table 13.

Table 14 shows the relative oxide composition of the blending components and of the four blends used in the simulations (Table 3). A water-to-binder (w/b) ratio of 0.5 was used throughout, and the simulations were made on a thermodynamically closed system (no mass loss or gain).

[64] Kulik, D.A.; Winnefeld, F.; Kulik, A.; Miron, G.D.; Lothenbach, B. CemGEMS—An easy-to-use web application for thermodynamic modelling of cementitious materials. RILEM Tech. Lett. 2021, 6, 36–52. https://doi.org/10.21809/rilemtechlett.2021.140.

Table 13 Slag and RGP glass phases equations for the reactive and unreactive phase.

Mix No.	Active/Inert Glass Phase
(50% slag)	$(SiO_2)_{6.0653}(Al_2O_3)_{0.9651}(Fe_2O_3)_{0.0494}(CaO)_{7.8955}(MgO)_{1.9639}(SO_3)_{0.0102}(K_2O)_{0.0478}(Na_2O)_{0.033}$ = + 6.0653 SiO_2 + 1.9302 AlO_2^- + 0.0988 FeO_2^- + 7.8955 Ca^{+2} + 1.9639 Mg^{+2} + 0.0102 SO_4^{-2} + 0.0956 K^+ + 0.066 Na^+ − 17.831 H^+ + 8.9155 H_2O
(34% slag)	$(SiO_2)_{6.0702}(Al_2O_3)_{0.9659}(Fe_2O_3)_{0.0494}(CaO)_{7.902}(MgO)_{1.9655}(K_2O)_{0.0479}(Na_2O)_{0.0331}$ = + 6.0702 SiO_2 + 1.9318 AlO_2^- + 0.0988 FeO_2^- + 7.902 Ca^{+2} + 1.9655 Mg^{+2} + 0.0958 K^+ + 0.0662 Na^+ − 17.8664 H^+ + 8.9332 H_2O
(6% RGP)	$(SiO_2)_{12.2273}(Al_2O_3)_{0.1307}(Fe_2O_3)_{0.0227}(CaO)_{2.8507}(MgO)_{0.4286}(K_2O)_{0.0566}(Na_2O)_{1.0634}$ = + 12.2273 SiO_2 + 0.2614 AlO_2^- + 0.0454 FeO_2^- + 2.8507 Ca^{+2} + 0.4286 Mg^{+2} + 0.1132 K^+ + 2.1268 Na^+ − 8.4918 H^+ + 4.2459 H_2O
(51% slag)	$(SiO_2)_{6.0702}(Al_2O_3)_{0.9659}(Fe_2O_3)_{0.0494}(CaO)_{7.902}(MgO)_{1.9655}(K_2O)_{0.0479}(Na_2O)_{0.0331}$ = + 6.0702 SiO_2 + 1.9318 AlO_2^- + 0.0988 FeO_2^- + 7.902 Ca^{+2} + 1.9655 Mg^{+2} + 0.0958 K^+ + 0.0662 Na^+ - 17.8664 H^+ + 8.9332 H_2O
(9% RGP)	$(SiO_2)_{12.2273}(Al_2O_3)_{0.1307}(Fe_2O_3)_{0.0227}(CaO)_{2.8507}(MgO)_{0.4286}(K_2O)_{0.0566}(Na_2O)_{1.0634}$ = + 12.2273 SiO_2 + 0.2614 AlO_2^- + 0.0454 FeO_2^- + 2.8507 Ca^{+2} + 0.4286 Mg^{+2} + 0.1132 K^+ + 2.1268 Na^+ − 8.4918 H^+ + 4.2459 H_2O

Table 14 Relative oxide composition of the materials and of the formulations simulated (shaded).

Composition of Paste Formulations			
Oxide	50% CEM II + 50% GGBS	60% GGBS + 40% RGP	40% GGBS + 60% RGP
SiO_2	26.79	27.02	29.28
CaO	52.86	53.07	50.73
MgO	5.15	4.267	4.69
Al_2O_3	6.88	5.83	6.25
Fe_2O_3	1.81	1.99	1.78
TiO_2	0.50	0.43	0.45
Mn_3O_4	0.20	0.20	0.19
Na_2O	0.22	0.58	0.67
K_2O	0.49	0.50	0.49
$CaCO_3$	5.24	6.29	5.24
Total	100.14	100.18	99.77

Red Mud models

As mentioned above, it was not possible to obtain red mud samples to measure oxide proportions and phase composition. However, using data from the literature[65] of red mud produced by the Bauer process, a thermodynamic model was developed for the study to demonstrate the hydration behaviour. The model consisted of a 90% CEM I + 10% red mud binder without any activator or other SCMs. The data used was taken from the literature and summarised in Table 15. Due to the additional aluminium, a C-A-S-H gel model was used using the DSPs in Table 9. The CEM was assumed to react using the Parrot and Killoh model[54]. While no data on the dissolution kinetics of the red mud was found, Equation 5 used for the PFA[63] was assumed. This is an area where more research is needed. 80% of the amorphous red mud was assumed to be reactive. Table 16 shows the derived thermodynamic equation to represent the glass phase of the red mud at the 10% replacement levels using the oxide proportions and phase compositions in Table 15.

To account for the rutile, anatase, perovskite, boehmite, diaspore and corundum phases that are not within the CEMDATA 18 database, additional input is needed to run the analysis. This is shown in Table 17 which is added to the SOLUTION_MASTER_SPECIES, SOLUTION_SPECIES and PHASES datablocks. This data is taken from the JAEA databse[59] and adjusted to suit PHREEQC.

[65] Hertel, T., Van den Bulck, A., Onisei, S., Sivakumar, P.P. and Pontikes, Y., 2021. Boosting the use of bauxite residue (red mud) in cement-Production of an Fe-rich calcium sulfoaluminate-ferrite clinker and characterisation of the hydration. Cement and Concrete Research, 145, p.106463.

Table 15 Chemical compositions and phase components of red mud taken from[65]

Oxide	wt.%	Phases	wt.%
SiO_2	9	Quartz	1
Al_2O_3	19.5	Calcite	5
Fe_2O_3	47.2	Hematite	37
CaO	11.6	Goethite	5
Na_2O	4.9	Gibbsite	5
TiO_2	6.2	Perovskite	6
LOI	9.7	Katoite	9
		Diaspore	14
		Rutile	1
		Boehmite	1
		Anatase	1
		Cancrinite	8
		Amorphous	7

Table 16 Red mud amorphous/glass phase equation for 10% replacement

$(SiO_2)_{1.5035}(Al_2O_3)_{1.5982}(Fe_2O_3)_{2.7078}(CaO)_{1.9799}(Na_2O)_{0.8024}(H_2O)_{5.3412}(TiO_2)_{0.7177}$ = + 1.5035 SiO_2 + 3.1964 AlO_2^- + 5.4156 FeO_2^- + 1.9799 Ca^{+2} + 1.6048 Na^+ + 0.7177 TiO_2 + 3.0474 H^+ + 3.8175 H_2O

Table 17 Additional thermodynamic data needed to run the red mud hydration analysis taken from[59]

SOLUTION_MASTER_SPECIES				
Ti	TiO2	0.0	Ti	47.8670
Cd	Cd+2	0.0	Cd	112.411
As	H2AsO4-	0.0	As	74.9216
Cr	CrO4-2	0.0	CrO4-2	51.9961
Pb	Pb+2	0.0	Pb	207.20
Pb(+2)	Pb+2	0.0	Pb	

SOLUTION_SPECIES		
TiO2	=	TiO2
log_k	0.0	
TiO2 + H2O	=	HTiO3- + H+
log_k	11.8041	
Cd+2	=	Cd+2
	llnl_gamma	
	5.0000	
	log_k 0	
	delta_H 0 kJ/mol	
H2AsO4-	=	H2AsO4-
	llnl_gamma	
	4.0000	
	log_k 0	
	delta_H 0 kJ/mol	
CrO4-2	=	CrO4-2
	llnl_gamma	
	4.0000	
	log_k 0	
	delta_H 0 kJ/mol	
Pb+2	=	Pb+2
	llnl_gamma	
	4.5000	

log_k 0
delta_H 0 kJ/mol

PHASES			
Rutile TiO2 + H2O = HTiO3- + H+ log_k	-20.7643	Boehmite AlO(OH) = AlO2- + H+ log_k	-15.2826
Anatase TiO2 + H2O = HTiO3- + H+ log_k	-19.79923656	Diaspore AlO(OH) = AlO2- + H+ log_k	-16.01478571
Perovskite CaTiO3 + H+ = Ca+2 + HTiO3- log_k	-2.626407361	Corundum Al2O3 + H2O = 2 AlO2- + 2 H+ log_k	-28.81671947

Geopolymer model

To model geopolymer cement hydration, discrete solid phases (DSPs) needed to be derived and included in the PHREEQC input files to consider the changing Ca/Si ratios. The CEMDATA 18 database[50] contains the eight end-members, which are listed in Table 18. It is anticipated that over 100 DSPs will be needed which is an area of ongoing research.

Table 18 CEMDATA 18[50] end-members to derive C-N-A-S-H DSPs

End-member	Thermodynamic equation	Log_k (@25^{0}C)
INFCA	$(CaO)_1(SiO_2)_{1.1875}(Al_2O_3)_{0.15625}(H_2O)_{1.65625} + 1.6875H^+ = Ca^{+2} + 0.3125AlO_2^- + 2.5H_2O + 1.1875SiO_2$	8.953727
TobH	$(CaO)_1(SiO_2)_{1.5}(H_2O)_{2.5} + 2H^+ = Ca^{+2} + 3.5H_2O + 1.5SiO_2$	12.797208
5CA	$(CaO)_{1.25}(SiO_2)_1(Al_2O_3)_{0.125}(H_2O)_{1.625} + 2.25H^+ = 1.25Ca^{+2} + 0.25AlO_2^- + 2.75H_2O + SiO_2$	15.88995
INFCNA	$(CaO)_1(SiO_2)_{1.1875}(Al_2O_3)_{0.15625}(Na_2O)_{0.34375}(H_2O)_{1.3125} + 2.375H^+ = 0.3125AlO_2^- + Ca^{+2} + 0.6875Na^+ + 2.5H_2O + 1.1875SiO_2$	17.23247
T5C	$(CaO)_{1.25}(SiO_2)_{1.25}(H_2O)_{2.5} + 2.5H^+ = 1.25Ca^{+2} + 3.75H_2O + 1.25SiO_2$	18.445467
INFCN	$(CaO)_1(SiO_2)_{1.5}(Na_2O)_{0.3125}(H_2O)_{1.1875} + 2.625H^+ = Ca^{+2} + 0.625Na^+ + 2.5H_2O + 1.5SiO_2$	18.759957
5CNA	$(CaO)_{1.25}(SiO_2)_1(Al_2O_3)_{0.125}(Na_2O)_{0.25}(H_2O)_{1.375} + 2.75H^+ = 1.25Ca^{+2} + 0.5Na^+ + 0.25AlO_2^- + 2.75H_2O + SiO_2$	23.240018
T2C	$(CaO)_{1.5}(SiO_2)_1(H_2O)_{2.5} + 3H^+ = 1.5Ca^{+2} + 4H_2O + SiO_2$	25.565334

5.2 Phase assemblage predictions

CEM I and CEM II / A-L

The predicted phase assemblages for the CEM I and CEM II / A-L model using the XRF input above are shown in Figure 26. As can be seen, the main difference in the two phase assemblages is the higher volume of calcite as expected in the CEM II / A-L cement. The AFm phase is monocarbonate, as predicted by Holmes *et al*[66]. Previous work[67,68,69] has shown that the formation of monosulphate, ettringite, hemicarbonate, monocarbonate and/or calcite is controlled by the available molar ratios of SO_3/Al_2O_3 and CO_2/Al_2O_3. The presence of calcite in both cements promoted the formation of monocarbonate and stabilised ettringite and the destabilisation of monosulphate.

The formation of hemicarbonate is sometimes observed in measured XRD data but not always predicted by thermodynamic modelling, reflecting its kinetic persistence experimentally. The dissolution of calcite is much higher than measured, which would further support the precipitation of monocarbonate over hemicarbonate due to the higher $CaCO_3$ content.

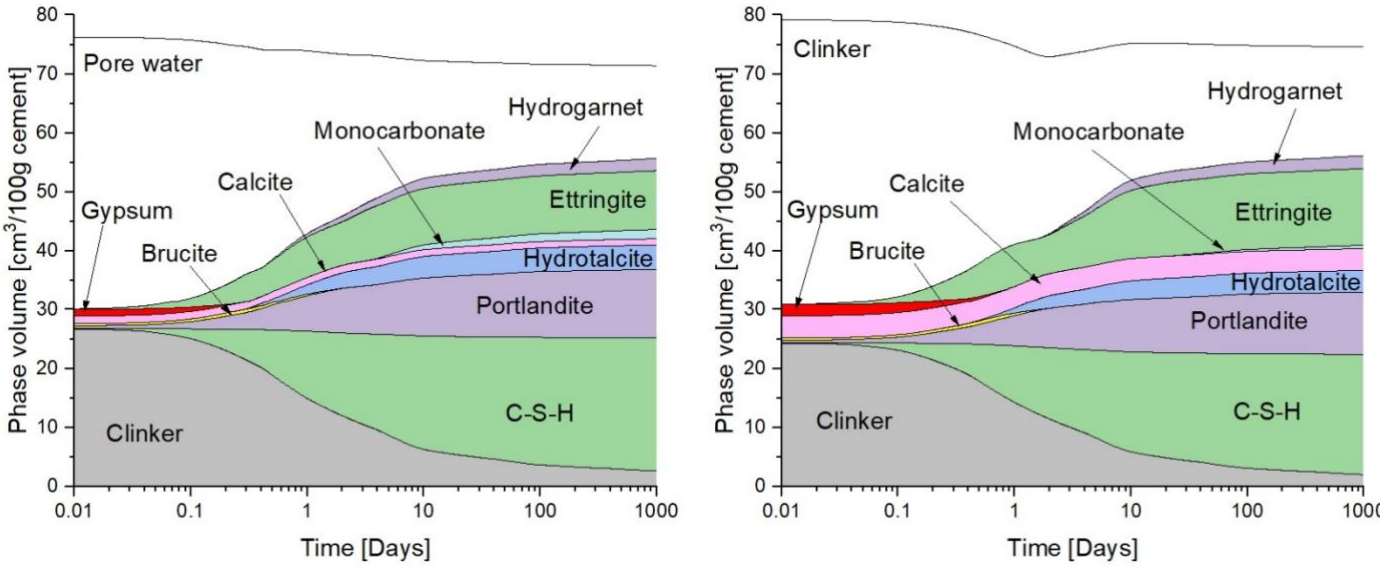

Figure 26 (a) CEM I and (b) CEM II / A-L phase assemblages

PFA

The change in the solid phase assemblage predicted by PHREEQC over time is shown in Figure 27. The results show the formation of monocarbonate with a stable ettringite phase, which agrees with the experimental observations. The formation of monocarbonate occurs at approximately 3-days which is evident in the XRD patterns above. Furthermore, with increasing PFA, the volume of monocarbonate increases which

[66] Holmes, N., Russell, M., Davis, G. & Tyrer, M. (2022) Comparing the Measured and Thermodynamically Predicted AFm Phases in a Hydrating Cement. Appl. Sci. 12, 10147. https://doi.org/10.3390/app121910147

[67] De Weerdt, K.; Haha, M.B.; le Saout, G.; Kjellsen, K.O.; Justnes, H.; Lothenbach, B. Hydration mechanisms of ternary Portland cements containing limestone powder and fly ash. Cem. Concr. Res. 2011, 41, 279–291. https://doi.org/10.1016/j.cemconres.2010.11.014.

[68] Lothenbach, B.; Damidot, D.; Marchand, T.; Matschei, T. Thermodynamic modelling: State of knowledge and challenges. Adv. Cem. Res. 2010, 22, 211–223.

[69] Matschei, T.; Lothenbach, B.; Glasser, F.P. The role of calcium carbonate in cement hydration. Cem. Concr. Res. 2007, 37, 551–558. https://doi.org/10.1016/j.cemconres.2006.10.013

is due to the additional calcium and aluminates being released into solution and precipitating. De Weerdt *et al*[29] showed that increasing PFA in blended cements results in faster OPC/CEM I reaction. Also confirmed is the reduction in portlandite as it reacts with the silicates, along with the additional alumina, to form additional C-A-S-H. Also, part of the additional aluminates will contribute additional ettringite and monocarbonate phases as the sulfate content is lower in high PFA blended cement.

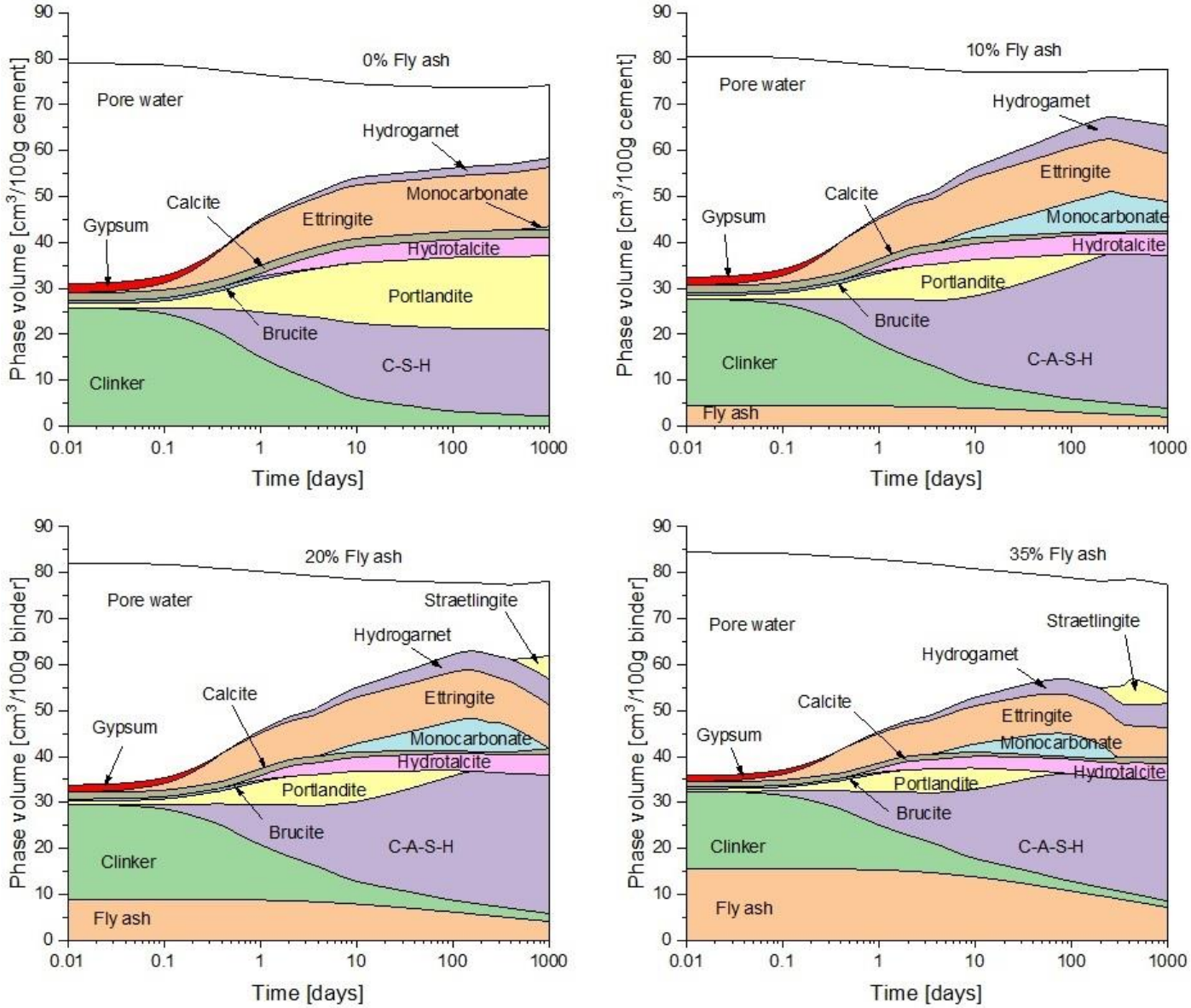

Figure 27 Phase assemblage changes over time for the 0, 10, 20 and 35% FA replacement levels.

FBA

The solid phase assemblage for the CEM I + 20% FBA over time is shown in Figure 28. The results are like the PFA binder but with reduced portlandite depletion due to the lower amorphous reactivity. This decreased pozzolanic behaviour is also seen in the compressive strength results which are lower across the 56 days compared to the PFA binder. This is an area where more focussed research is needed to truly understand the reactivity of the FBA at Moneypoint.

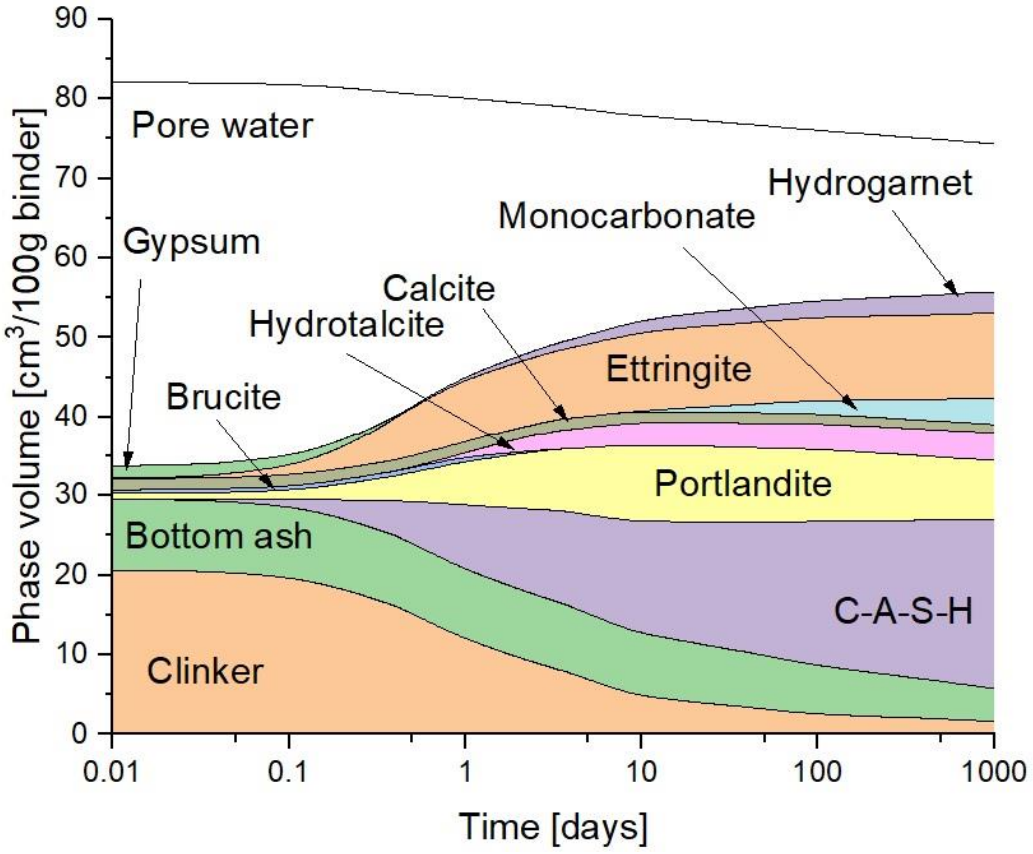

Figure 28 Phase assemblage for the 80% CEM I + 20% FBA blend

GGBS

The phase assemblage for the 50-50 CEM II / A-L and GGBS is shown in Figure 29. The phase assemblage is like the fly ash systems as portlandite is destabilised due to pozzolanic reactions. At higher replacement levels, increasingly portlandite would be converted to C-A-S-H with less monocarbonate. The presence of portlandite, C–A-S–H, ettringite, AFm (monocarbonate) and hydrotalcite phases have been observed in hydrated PC–slag systems[70].

RGP

The 40% RGP blend and 60% RC blends are shown in Figure 30. There is a difference in the final (1,000 day) phase quantities between the RGP blends and the 50-50 CEM II / A-L + GGBS paste. In each case, the solution chemistry is dominated by sodium and potassium, calcium, silicate, carbonate and sulphate as the next most abundant dissolved ions. For each ion in solution, the variation in predicted concentration between each blended cement is not significant.

[70] Lothenbach, B., Scrivener, K. and Hooton, R.D., 2011. Supplementary cementitious materials. Cement and concrete research, 41(12), pp.1244-1256.

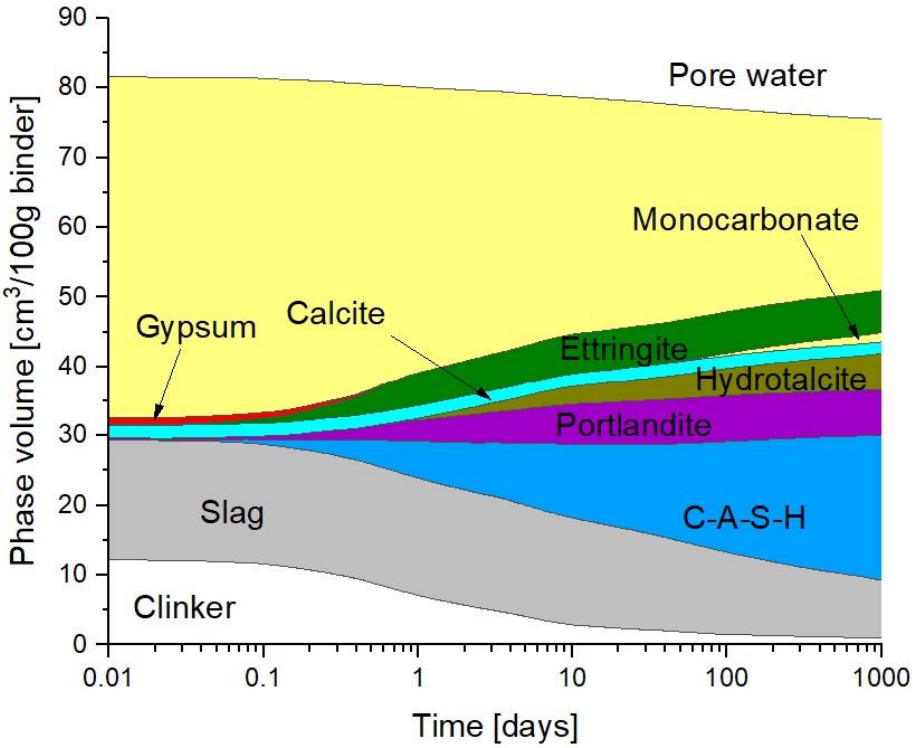

Figure 29 Phase assemblage for the 50% CEM II / A-L + 50% GGBS blend

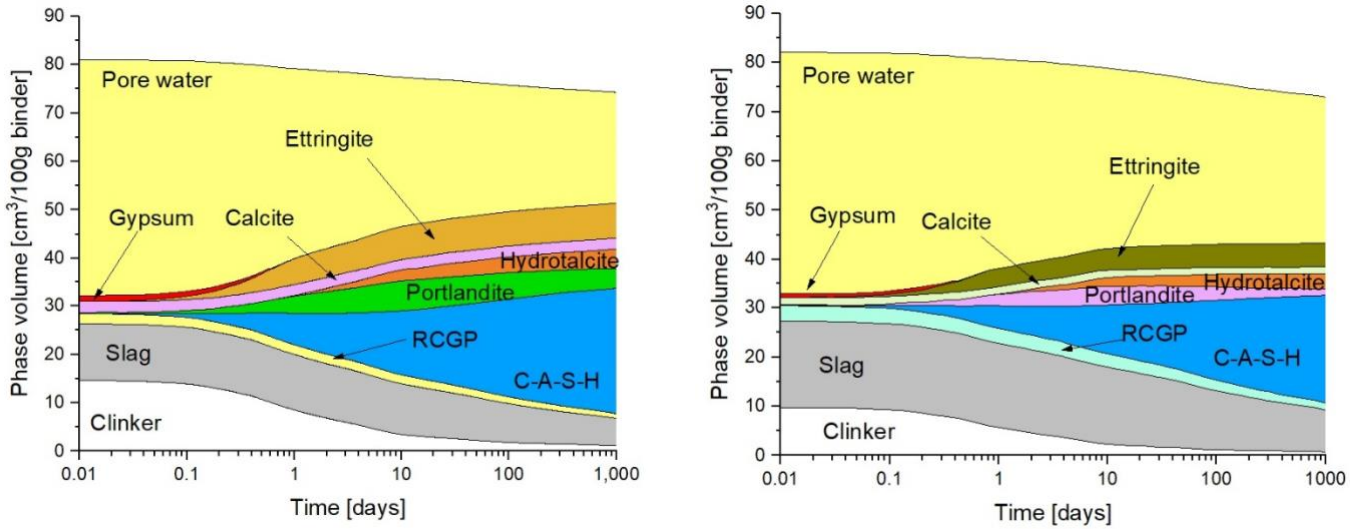

Figure 30 (a) 40% RGP and (b) 60% RGP blends

Calcined Clay

Figure 31 shows the expected phase assemblage at full hydration obtained by thermodynamic modelling for the LC3 system in this study. This system consisted of 55% OPC, 28% calcined clay, 15% limestone and 2% gypsum, at a w/b of 0.5. The phase assemblage was computed for different amounts of calcined clay from 0 to 30%. As shown, portlandite is totally consumed for around 15% (g/g binder) of calcined clay. Monocarbonate appears to increase up to 10% but decreases as stratlingite begins to precipitate. Ettringite content remains constant over the whole range simulated, as does calcite and hydrotalcite.

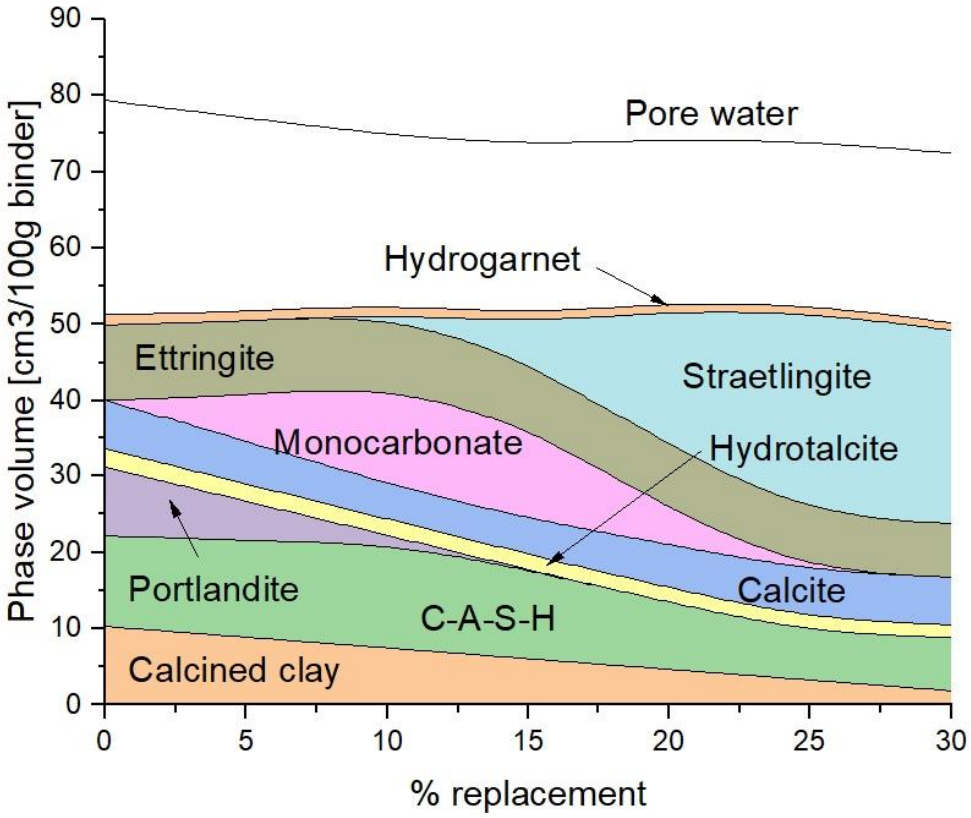

Figure 31 Phase assemblage for the Calcined clay cements

Red mud

The phase assemblage for the CEM I + 10% red mud binder is shown in Figure 32. As shown, the phase development is like a normal CEM I cement with the precipitation of C-A-S-H, portlandite, etc. It does not appear that pozzolanic behaviour is occurring as the volume of portlandite seams constant after 10 days. This may be due to the combination of the low amount of red mud used in the analysis and the small proportion of amorphous/glass in the sample, as shown in Table 15. The red mud phases (quartz, hematite, rutile, etc.) contribute very little to the overall volume and are only trace elements. Experimental observations of the phase development through XRD analysis must be undertaken to validate these predictions. However, it would appear on the face of it that red mud, albeit at low cement replacement levels, is not detrimental to cement hydration. Much more work is needed in this area to validate the assumptions made above.

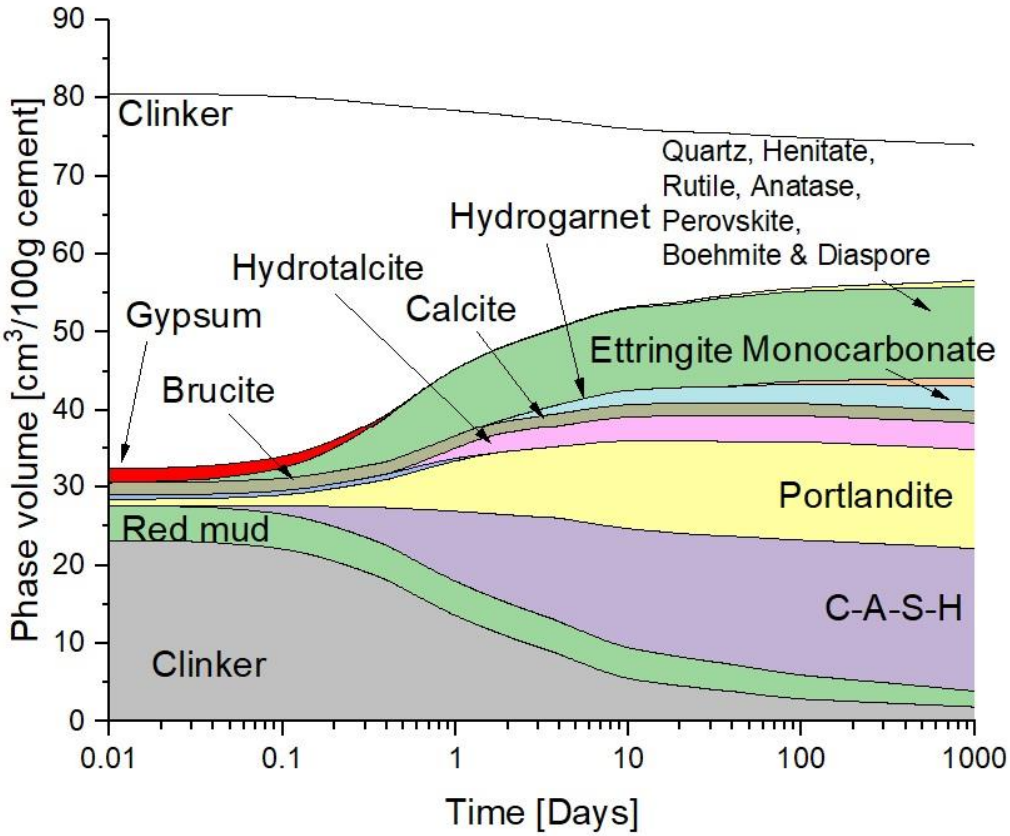

Figure 32 Phase assemblage for the 90% CEM I + 10% red mud binder

6 Route to standardisation

One of the important aspects of developing any new SCM is how it can be added to standards that are acceptable to the construct industry. This project aimed to develop a roadmap in consultation with the NSAI to enable new SCMs can be standardised for use in Ireland. To this end, a meeting was held on 9th September 2025 with Joseph Byrne from the NSAI and Brian O'Rourke, chairperson of the NSAIs Concrete Standards Consultative Committee, which is responsible for Irish national standards relating to concrete and related products.

The aim if the meeting was to discuss the development of a roadmap for standardizing new cement products in Ireland, review ongoing research, identify gaps in standards, and explore potential funding and collaborations. The meeting focused on standardising new cement products in Ireland, particularly alternative binders such as PFA, FBA, calcined clays and recycled glass powder. The discussion addressed ongoing research, current European and national standards and potential funding opportunities.

There is a lot of work ongoing in terms of reviewing and updating current standards. The Irish national annex to IS EN 206[46] is under review, with three draft standards published. A 12-month timeline has been set for completion of this work. Help will be required to draft national provisions and establish values for new binder types.

The challenges in standardising new cements were also discussed in detail. While existing standards cover certain supplementary materials like GGBS, fly ash and silica fume, there is no established framework for new binders without European input. Therefore, developing a standardised pathway for testing and approval of new binders remains a major challenge. To help overcome these challenges, and to prepare for the next revision of EN206, the Department of Enterprise, Tourism and Employment (DETE) with the support of the NSAI have sought separate Requests for Quotations (RFQs) to undertake the following projects:

- limiting values of composition and the durability performance of concretes used in Ireland
- identify the principles of a national approach to the General Suitability for Novel Cementitious Materials within the Concrete Standards and provide research and reports, and
- identify the principles of a national approach to evaluate the Specific Suitability for Novel Cementitious Materials within the Concrete Standards and provide research and reports.

While ongoing research into novel SCMs is active in academic institutions, increased collaboration with industry will provide mutual benefits and accelerate development of standards with the importance of long-term durability testing and performance evaluation of new materials emphasised.

In terms of future steps and increased collaboration, the establishment of a dedicated centre for standardising new cements was proposed, which could be commercially or state supported. This could have the facilities for site-based, long-term testing to assess durability and performance in the field. The Centre would nurture academic and industry collaboration on research projects and sharing expertise to encourage the development of standards. While the NSAI can manage outputs from research projects, it does not conduct research itself.

The key takeaways from the meeting are summarised below:

- A roadmap for the standardisation of new SCMs does not currently exist
- The assessment of alternative binders and addressing gaps in current knowledge is crucial if Ireland wants to reduce its carbon load from the production of traditional cement
- Collaboration between academic institutions, industry and government bodies is crucial.
- Ongoing ways to continue research in this area is vital including exploring follow-on funding streams

with collaboration at the core

- An emphasis on durability testing, performance evaluation and alignment with European standards is essential for the roadmap to succeed.

7 Discussion and Conclusions

Cement, and its use in concrete, is essential to modern infrastructure but it comes with a high environmental cost. The manufacture of Portland cement is highly carbon-intensive due to the calcination of limestone to produce clinker which involves the combustion of fossil fuels in kilns at extremely high temperatures. The resulting CO_2 emissions are responsible for approximately 8% of global values. In Ireland, the challenge to reduce embodied carbon is mirrored in national climate commitments and policy changes aimed at the construction industry. Reducing emissions from cement is therefore both an industry and regulatory priority.

As part of efforts to decarbonise public procurement, regulations now require state-funded projects in the Republic of Ireland to use "*low-carbon concrete*" which is defined as cement with a minimum clinker replacement level of 30% using lower-carbon materials. This mandate is intended to accelerate market adoption of alternative materials, reduce the carbon footprint of public infrastructure and spur the construction industry to use innovative and scale low-emission binders. Thankfully, this is not uncommon in Ireland but more can be done with new SCMs, which is the focus of this work.

SCMs or "*alternative cement materials*" generally refers to low-clinker binders that replace a portion of traditional OPC clinker in concrete. These materials often originate from industrial by-products or other processes that would otherwise be waste and have lower embodied carbon due to reduced energy requirements and avoided emissions. The most common SCM used in Ireland is GGBS with up to 70% cement replacement for particular applications. As shown in this study, other SCMs are available on the island such as PFA, limestone, recycled glass, FBA and calcined clays. Other than limestone, the availability of these materials are somewhat limited. Geopolymer cements, activated by alkaline solutions, offer ultra-low clinker content and corresponding emission reductions.

7.1 Experimental findings

The results from the experimental and thermodynamic analysis suggests that all SCMs in this study performed well. Compared to the CEM I and CEM II / A-L cements, the PFA samples performed best. Only relatively minor differences in strength (~10MPa) were observed in the GGBS, calcined clay and 6% RGP concretes. Higher differences were observed in the 9% RGP and FBA results (~20MPa) over the time-frames. Over longer time periods, these would be expected to increase.

The XRD patterns all demonstrate the precipitation of major phases including portlandite, ettringite and some AFm. There is evidence of portlandite reduction in the PFA, FBA, GGBS, RGP and calcined clay that demonstrate its conversion to additional C-(A)-S-H which contribute to higher strengths over time. This is further shown in the thermodynamic predictions where no observable reduction in volume is shown for all SCMs here.

7.2 Challenges, Considerations and the Path Forward

While GGBS has been a staple SCM in Ireland, its availability is tied to the steel industry, which itself is decarbonising and reducing blast furnace operations. Similarly, fly ash supply is diminishing globally with the phasing out of coal power, posing long-term supply challenges unless alternative sources or new SCMs are developed. Engineering standards and specifications have historically been oriented towards traditional OPC chemistry. New materials such as calcined clays and geopolymers often face regulatory and certification barriers before widespread adoption in structural applications. Research initiatives in Ireland aim to create performance frameworks to overcome such hurdles. Implementing alternative cement systems requires specialised technical knowledge in cement chemistry, hydration behaviour, mix design, curing conditions and quality control. This necessitates industry training and knowledge sharing between academic institutions,

Standards bodies, suppliers, contractors and engineers. New sustainable solutions in the cement and concrete space are being developed. These include Ecocem's ACT technology, Kilsaran's ClimaKrete and Techrete's recently launched range of sustainable concretes with reduced embodied carbon content.

The cement industry is classified as "*difficult to decarbonise*" in technical and technoeconomic assessments[71], and the reasons for this are both complex and deep-seated. Provis[72] suggests a four-fold classification to drive the production of sustainable cements and concrete including making better cement, making better concrete, making concrete better and using concrete better. Marandi and Shirzad[73] listed several dozen cement alternatives that are all worth further investigation using waste materials that are available in Ireland including calcium aluminate cements, calcium sulfoaluminate cements, magnesium-based cements and alkali-activated binders that offer lower CO_2 emissions by utilizing innovative chemical compositions and production methods.

New SCMs, non-traditional cements, novel binders and alternative binder cements to those found in IS EN 197[17] all offer significant potential in reducing embodied carbon. However, there is no structured national process for assessing these systems in Ireland. The Irish Annex to IS EN 206[46] depends on materials specified to harmonised standards. While the draft prEN 206-1 Clause 6 provides an option to establish suitability for a constituent, there is currently no process or framework in place for assessing novel cementitious materials. This is the focus of recent Requests for Quotations issued by The Department of Enterprise, Tourism and Employment (DETE) with the support of the NSAI to investigate (1) limiting values of composition and the durability performance of concretes used in Ireland, produce principles of a national approach to the (a) general suitability and (b) evaluation for novel cementitious materials within the concrete standards.

Concrete and cement are central to infrastructure and will continue to form an integral part of all our lives[74]. Collaboration between industry, academia and government is stronger than ever, and green public procurement policies are driving demand for a lower carbon and sustainable practical and scalable product. With the right investment and public awareness, concrete can be part of the climate solution. The story of cement, concrete and carbon is one of opportunity. Every bridge, school and home built with lower-carbon concrete brings us closer to more sustainable world for thousands of years to come.

[71] Davis, S.J., Lewis, N.S., Shaner, M., Aggarwal, S., Arent, D., Azevedo, I.L., Benson, S.M., Bradley, T., Brouwer, J., Chiang, Y.M. and Clack, C.T., 2018. Net-zero emissions energy systems. Science, 360(6396), p.eaas9793.

[72] Provis, J.L., 2025. Perspectives on research directions in cement and concrete. Journal of Asian Concrete Federation, 11(4), pp.1-13.

[73] Marandi, N. and Shirzad, S., 2025. Sustainable cement and concrete technologies: A review of materials and processes for carbon reduction.

[74] https://www.rte.ie/brainstorm/2025/0917/1531850-carbon-impact-cement-concrete-supplemental-cementitious-materials/

Construct Innovate
Built Environment Research Ireland

TECHNOLOGY CENTRE
ENTERPRISE IRELAND
IDA IRELAND SUPPORTED

Ollscoil na Gaillimhe
University of Galway

Trinity College Dublin
Coláiste na Tríonóide, Baile Átha Cliath
The University of Dublin

UCC
University College Cork, Ireland
Coláiste na hOllscoile Corcaigh

UCD DUBLIN

IGBC
IRISH GREEN BUILDING COUNCIL

In support of Project Ireland 2040 and the work of the Construction Sector Group Innovation and Digital Adoption Sub-Group